Extreme rainfall variability in Australia: Patterns, drivers and predictability

Article

Accepted Version

Title: Extreme rainfall variability in Australia: Patterns, Drivers, and Predictability

Authors: Andrew D. King[1,2], Nicholas P. Klingaman[3], Lisa V. Alexander[1,2], Markus G. Donat[1,2], Nicolas C. Jourdain[2], and Penelope Maher[1,2]

1. ARC Centre of Excellence for Climate System Science, University of New South Wales, Sydney, NSW, Australia.

2. Climate Change Research Centre, University of New South Wales, Sydney, NSW, Australia.

3. National Centre for Atmospheric Science and Department of Meteorology, University of Reading, Reading, United Kingdom.

Corresponding Author: Andrew D. King, Climate Change Research Centre, Level 4, Mathews Building, University of New South Wales, Sydney, NSW, 2052, Australia.

Email: andrew.king@student.unsw.edu.au

Date of original submission: 24th November 2013

Date of re-submission: 24th March 2014

Extreme rainfall variability in Australia: Patterns, drivers, and predictability

Andrew D. King, Nicholas P. Klingaman, Lisa V. Alexander, Markus G. Donat, Nicolas C. Jourdain, Penelope Maher

Abstract

Leading patterns of observed monthly extreme rainfall variability in Australia are examined using an Empirical Orthogonal Teleconnection (EOT) method. Extreme rainfall variability is more closely related to mean rainfall variability during austral summer than in winter. The leading EOT patterns of extreme rainfall explain less variance in Australia-wide extreme rainfall than is the case for mean rainfall EOTs. We illustrate that, as with mean rainfall, the El Niño-Southern Oscillation (ENSO) has the strongest association with warm-season extreme rainfall variability, while in the cool-season the primary drivers are atmospheric blocking and the subtropical ridge. The Indian Ocean Dipole and Southern Annular Mode also have significant relationships with patterns of variability during austral winter and spring.

Leading patterns of summer extreme rainfall variability have predictability several months ahead from Pacific sea surface temperatures (SSTs) and as much as a year in advance from Indian Ocean SSTs. Predictability from the Pacific is greater for wetter than average summer months than for months that are drier than average, whereas for the Indian Ocean the relationship has greater linearity.

Several cool-season EOTs are associated with mid-latitude synoptic-scale patterns along the south and east coasts. These patterns have common atmospheric signatures denoting moist onshore flow and strong cyclonic anomalies often to the north of a blocking anti-cyclone.

Tropical cyclone activity is observed to have significant relationships with some warm season EOTs.

This analysis shows that extreme rainfall variability in Australia can be related to remote drivers and local synoptic-scale patterns throughout the year.

1. Introduction

Rainfall in Australia is highly variable, both temporally and spatially, to a greater degree than in other countries and continents (Nicholls et al. 1997). This strong interannual variability is related to a variety of climate modes of variability including the El Niño-Southern Oscillation (ENSO), Indian Ocean Dipole (IOD), and the Southern Annular Mode (SAM). We discuss here relationships between these climate modes and Australian rainfall variability from previous literature. A map of the states and territories of Australia mentioned here is shown in Figure 1.

The effects of ENSO on Australian rainfall variability are well documented (e.g. Allan 1988; McBride and Nicholls 1983; Nicholls et al. 1996). ENSO is generally considered to be the primary driver of rainfall variability in Australia. Rainfall in the east of Australia has the strongest relationship with ENSO (Risbey et al. 2009), where La Niña (El Niño) events are associated with increased (decreased) rainfall. ENSO also influences the summer monsoon, affecting rainfall patterns in northern Australia (Holland 1986). The position of the South Pacific Convergence Zone (SPCZ) is influenced by ENSO (Brown et al. 2011; Vincent et al. 2011), affecting rainfall patterns in north-east Australia and the locations of tropical cyclogenesis (Vincent et al. 2011). The ENSO-rainfall relationship is non-linear across Australia generally (Power et al. 2006) and within specific regions such as south-east Queensland (Cai et al. 2010) and south-east Australia (King et al. 2013c), whereby the impact of ENSO on rainfall during La Niña events is stronger than during El Niño events.

The IOD primarily modulates rainfall on inter-annual timescales in western and southern Australia during winter and spring (Risbey et al. 2009). The IOD is also related to the climate of south-east Australia (Meyers et al. 2007) and has been linked to droughts in this region (Ummenhofer et al. 2009; Ummenhofer et al. 2011).

Unlike ENSO and the IOD, SAM is an extra-tropical mode that reflects variability in the Southern Hemisphere mid-latitude storm tracks (Marshall 2003). Consequently it is associated with rainfall in southern Australia, such as south-west Western Australia and parts of south-east Australia (Meneghini et al. 2007; Risbey et al. 2009). The SAM is also related to spring rainfall in Queensland and New South Wales through teleconnections with weather systems located over the Tasman Sea (Hendon et al. 2014; Risbey et al. 2009). A positive trend in the SAM in recent decades has been associated with the rainfall decline in south-west Western Australia (Cai and Cowan 2006; Meneghini et al. 2007). Other studies suggest a weaker teleconnection between SAM and south-west Western Australia rainfall (Feng et al. 2010).

Several studies have considered how some of these remote drivers relate to mean and extreme rainfall variability in Australia as a whole (e.g. Risbey et al. 2009; Min et al. 2013) and within particular regions of the continent (e.g. Gallant et al. 2012; Klingaman et al. 2013). The relative roles of these remote drivers are examined in this study.

Australian climate is also influenced by many local drivers. Atmospheric blocking to the southeast of Australia is known to increase rainfall over much of Australia, particularly during the cool season (Risbey et al. 2009). The position and intensity of the subtropical ridge influences rainfall in the east of Australia (Cai et al. 2011; Timbal and Drosdowsky 2013; Whan et al. 2013). An important consideration when investigating the effects of these remote and local drivers on Australian climate is the lack of independence between drivers.

Weather and climate regimes vary across Australia. The north of the country has a tropical/subtropical climate with the majority of rainfall concentrated during the summer months. Monsoon depressions and tropical cyclones are the major rain-bearing systems in this region. The extra-tropical south of Australia is affected by mid-latitude frontal systems. East Coast Lows affect the coasts of Victoria and New South Wales, bringing rainfall in winter primarily. The south and south-west experience more rainfall in winter, whereas, in the south-east, rainfall is more consistent through the year. These weather systems are affected by the remote and local drivers described previously in complex and sometimes conflicting ways, complicating the study of rainfall variability in Australia.

The effects of these modes of variability and different weather systems on continental and regional rainfall have been studied to some degree. However, there has been less focus on the relationships between climate drivers and extreme rainfall. Therefore, further analysis of the associations between rainfall and different climate modes is required. These relationships may well differ from those that have been studied previously for mean rainfall. Extreme rainfall has the greatest impact on people and the environment. Very heavy rainfall can lead to severe floods, such as those of 2010-11 that devastated large areas of Queensland. Improving our understanding of the regional effects of drivers of extreme rainfall would be beneficial and may lead to improved seasonal predictability of flooding. For example, it is understood that extreme rainfall is heavier during La Niña events than in neutral or El Niño events (e.g. King et al. 2013a). However, there are gaps in our scientific understanding of how teleconnections between ENSO (and other climate drivers) and extreme rainfall vary monthly and seasonally.

A limited number of studies have examined the statistical relationships between modes of variability and extreme rainfall in Australia, but few have considered physical mechanisms. Min et al. (2013) examined the statistical relationships between ENSO, SAM, and the IOD with extreme rainfall, calculated using extreme value statistics. Strong relationships exist between ENSO and extreme rainfall in eastern Australia with multi-decadal modulation related to the Interdecadal Pacific Oscillation (IPO) (King et al. 2013a).

This study aims to analyze patterns of extreme rainfall variability across Australia and relationships with mean rainfall, climate modes of variability, and the activity of several weather system types. Comparisons are made between results for extreme and mean rainfall to examine differences in relationships. Predictability of extreme (and mean) rainfall patterns is also considered in this study.

A brief description of the data used and the methods applied is outlined in section 2 (more details on the methodology can be found in the Supplementary material). Results are presented for each climate driver or weather system type and are described in section 3. A discussion of the results and the conclusions is given in section 4.

2. Data and Methods

The observational monthly total and extreme precipitation data used in this study were calculated from the Australian Water Availability Project (AWAP) gridded dataset of daily rainfall (Jones et al. 2009). The AWAP dataset runs from 1900 to the present and grids all available station data on a particular day on to a 0.05^{o} grid. The data were regridded to a 0.5^{o} resolution for computational reasons. The impacts of using data of different horizontal resolutions were tested and found to have minimal effects on the results. As an aim of the study was to look at spatial variability of total and extreme rainfall, a gridded product was deemed more appropriate than station data. Over most of Australia, AWAP captures extreme rainfall variability, however, in some rural areas, where the station network is sparse, the gridded data have spurious trends (King et al. 2013b), therefore a mask was applied. For our study, areas of Australia where AWAP has any missing values during the analysis period were masked. To limit issues of variability in the station network used to generate AWAP, analysis was limited to 1930-2011. Prior to 1930 there were fewer stations used in the calculation of the AWAP daily rainfall grids (Jones et al. 2009). Results found using AWAP were evaluated against those using other rainfall datasets (see Supplementary Material for more details).

In this study, extreme rainfall is defined using the monthly maximum consecutive 5-day precipitation totals (Rx5day hereafter). This is an extreme rainfall index recommended by the Commission for Climatology (CCI)/CLIVAR/JCOMM Expert Team on Climate Change Detection and Indices (ETCCDI; Zhang et al. 2011). The total rainfall and Rx5day index were calculated for each 0.5^{o} gridbox in each month of the 82-year period. Only AWAP gridboxes where the time series of the total rainfall and Rx5day index were complete (i.e. with no missing data) were used in this investigation.

To examine spatial and temporal variability in the monthly rainfall and Rx5day across Australia, an Empirical Orthogonal Teleconnection (EOT; van den Dool et al. 2000) method was applied. A detailed description of the method and its verification is in the Supplementary Material section. In short, EOT analysis statistically decomposes the (extreme) rainfall fields into orthogonal (in time) time series related to the spatial points that explain the greatest space-time variance in the domain (as measured by correlation coefficients with all other gridboxes). That is, there is one grid point (referred to as the base point) that is associated with the greatest amount of variance across all other gridpoints. The orthogonality of the EOTs allows for the investigation of multiple drivers of Australian (extreme) rainfall variability beyond the primary driver. EOTs are only orthogonal in either time or space, whereas Empirical Orthogonal Functions (EOFs) are orthogonal in both time and space, making the physical interpretation of EOTs simpler than EOFs. We calculate EOTs that are orthogonal in time. A modified EOT method (Smith 2004) using the all-Australia mean (and extreme) rainfall time-series, as opposed to the global variance, was applied. Use of the global variance biases results to regions of higher rainfall totals. The modified EOT method applied in this study more naturally lends itself to studying mean (and extreme) rainfall variability.

As many EOTs can be computed as are desired (up to the number of gridboxes in the domain). After the first EOT, the calculation is repeated on residual time-series that remove, by linear regression, the effects of EOTs calculated previously. The first four EOTs were calculated separately for each calendar month of the 1930-2011 timeseries for Rx5day and total rainfall to allow for the investigation of several extreme and mean rainfall patterns across different regions of Australia. EOTs were also calculated using seasonal data, but these EOTs missed some details that were better captured with monthly analysis, such as the annual cycle of the ENSO influence on extreme rainfall.

2.1. Indices for remote drivers

Indices for several climate drivers were used to examine statistical relationships with EOTs. ENSO is represented by the Southern Oscillation Index (SOI) and the Niño-3.4 SST Index, so that both atmospheric and oceanic indices were considered. The SOI was calculated as the difference in standardized mean sea-level pressure between Tahiti and Darwin (Trenberth et al. 1984). The Niño-3.4 index was calculated from the HadISST dataset as an SST-based index of ENSO (Rayner et al. 2003). The IOD is represented by the Dipole Mode Index (DMI; Saji et al. 1999) also calculated from HadISST. The DMI was both correlated and partially correlated (removing ENSO influence) with EOTs. The SAM index (SAMI) is that of Marshall (2003) and was calculated using station-based data as the difference in pressure between 40^{o}S and 65^{o}S (Gong and Wang 1999). The relationship between the SAM and the

EOTs was examined for the 1957-2011 period of reliable SAM data (Marshall 2003). Timeseries of the indices described here are shown in Figure S1.

Relationships between the Interdecadal Pacific Oscillation (IPO) and EOT time series were also analyzed as previous studies have found relationships between the IPO and total (Power et al. 2006; Klingaman et al. 2013; Speer 2008; Speer et al. 2011) and extreme rainfall (King et al. 2013a) in parts of eastern Australia particularly. All correlations between an index for the IPO (Parker et al. 2007) and EOT time series were found to be non-significant after reduction in the number of degrees of freedom to account for serial interannual persistence in the IPO. The Madden-Julian Oscillation (MJO; Madden and Julian 1971) is an important driver of Australian rainfall variability. The MJO was not considered in this study as it is an intraseasonal mode of variability which would require (extreme) rainfall indices at a daily or weekly resolution as opposed to the monthly indices applied in this study.

To examine the physical mechanisms behind mean and extreme rainfall variability, reanalysis fields were used. The Twentieth Century reanalysis (20CR hereafter; Compo et al. 2011) extends further back in time than other reanalysis products, to 1871 (before the start date of this study's analysis). The reanalysis was generated through using an atmosphere-only model constrained by observed surface pressure, sea surface temperatures (SSTs) and sea ice. An ensemble of 56 members was generated using an Ensemble Kalman filter data assimilation technique. King et al. (2013a) found that the 20CR ensemble members captured the observed ENSO-extreme rainfall relationship in eastern Australia, suggesting that it performs reasonably well in this region. Ensemble-mean 20CR fields have been used to examine Queensland rainfall variability (Klingaman et al. 2013) and climate variability in southeast Australia (Ashcroft et al. 2013). The 20CR fields used in this study are outgoing longwave radiation, mean sea level pressure (MSLP), zonal and meridional winds, and specific humidity. All 20CR data used here have a monthly resolution and are the ensemble-mean fields.

2.2. Indices for local drivers

Indices calculated from the 20CR (for the period 1930-2010) were also used to represent variability in large-scale systems that affect Australian weather. The atmospheric blocking index (BI) was calculated using 20CR 500 hPa zonal winds (Pook and Gibson 1999). For points along 140^{o}E, the BI is defined as:

$$BI = 0.5(U_{25} + U_{30} - U_{40} - 2U_{45} - U_{50} + U_{55} + U_{60})$$

where U_x is the monthly-mean zonal wind at each latitude "x" in the Southern Hemisphere.

Indices for the position and the intensity of the subtropical ridge (STR-P and STR-I respectively; Larsen and Nicholls 2009) were calculated from 20CR MSLP by cubic spline fitting of the zonally averaged MSLP across the Australian domain (10^{o}S-50^{o}S, 110^{o}E-155^{o}E). The maximum of the spline fit gives the STR-I index, and the latitude at which the maximum occurs gives the STR-P.

The position of the western portion of the South Pacific Convergence Zone (SPCZ) is represented by an index (SPCZ-I; Vincent et al. 2011). This index was calculated from 20CR precipitation as the latitude of maximum zonally averaged precipitation between 155^{o}E and 175^{o}E.

Indices for tropical cyclone frequency were also calculated using observed tracks from the IBTrACS dataset (Knapp et al. 2010). Monthly indices of cyclone frequency (TC-E and TC-W for eastern and western regions respectively), were calculated by counting the number of cyclones per day that pass through two defined regions (shown in Figure 5) in each month of the warm season (November-April) from 1930-2010.

The time series of these local indices are also shown in Figure S1. All indices were correlated or partially correlated (removing ENSO using the Niño-3.4 index) with EOT time series. Correlations (Spearman's rank) are defined as statistically significant at the 5% level (p-value < 0.05). Given that correlations are calculated between each climate index and 96 EOTs (four for each calendar month for both total and extreme rainfall), and the 5% significance level applied, approximately five of these correlations would be expected to be significant by chance for each climate mode. Therefore, caution needs to be exercised in the analysis based on these correlation coefficients.

All correlations between climate indices and the EOT time series are Spearman's rank. This is because several indices, including the tropical cyclone indices, are not normally distributed. Nevertheless, tests showed high agreement between Pearson's and Spearman's rank correlation coefficients for the majority of climate indices. The fields were correlated with, and regressed onto, individual EOTs to produce maps.

3. Results

3.1 EOT correlation maps

The EOTs were calculated for the Rx5day index (and total rainfall) for each month of the year over 1930-2011. The base point of an EOT is the grid point which has the time series that explains the most variance in time series at other points. Correlating the base point time series of each EOT with the time series at other grid points gives an idea of the spatial variance in extreme (and total) rainfall. Maps of these correlation coefficients were plotted for each EOT. Examples for the leading EOTs of January and August extreme and mean rainfall are shown in Figure 2.

The locations of the base points of the leading EOTs shift seasonally for both extreme and total rainfall (Fig. 2 and S2). The base points for extreme and total rainfall are in similar locations during the warmer months, in the north and north-east of Australia. In the cooler months the locations of leading Rx5day EOTs tend to move polewards, but more so for total rainfall. This is particularly clear in August (Fig. 2 and S2c) and October (Fig. S2e) where the leading total rainfall EOTs are in Victoria and SE New South Wales, respectively. Although, in other cool season months, such as July (Fig. S2b) and September (Fig. S2d), the leading EOTs of extreme and total rainfall are in similar locations. However, the second-order EOTs of total rainfall in July and September are located much further south than those of extreme rainfall. There is greater variability in the locations of lower-order EOTs generally.

All of the 48 extreme rainfall EOT basepoints (four EOTs for each of 12 months) are on mainland Australia, however three cool season EOTs of monthly total rainfall are located on Tasmania. The total space-time variance associated with the first four EOTs varies from month-to-month, but has a stronger seasonal cycle for extreme rainfall than for total rainfall (Fig. S3; Tables S1, S2). In the cool season there appears to be greater spatial homogeneity in extreme rainfall than in the warm season, with more widespread coherent extreme rainfall patterns. In all months there is lower variance in extreme rainfall explained by the four leading extreme rainfall EOTs than total rainfall variance explained by the first four total rainfall EOTs.

The space-time variance associated with each Rx5day EOT is between 8% and 22% for each leading EOT and decreases for lower-order EOTs to a minimum of roughly 4% when studying at the first four EOTs for each month. These values are lower than those found for monthly total rainfall, and considerably lower than those found with EOTs of seasonal rainfall in Queensland (Klingaman et al. 2013) and annual rainfall nationally (Smith 2004). One possible explanation for this may be increased inhomogeneities in monthly extreme rainfall as opposed to monthly, seasonal, and annual total rainfall, leading to less coherent variability. Also, the Australia domain examined in this study is large compared with Queensland (the focus of Klingaman et al. (2013)). Explained variance would be expected to decrease with increases in domain size as different areas of Australia have different relationships between modes of variability and extreme rainfall. Smith (2004) found the leading EOT of annual rainfall, located in SW Queensland, was associated with 60% of variance. A similar calculation of the leading annual rainfall EOT in AWAP, with a mask applied, found this EOT to be located further north-east and associated with only 25% of space-time variance across Australia (not shown). However, Smith (2004) used the SILO gridded dataset (Jeffrey et al. 2001) without the application of a mask through central areas of Australia where there are few rainfall stations. In these areas, over-smoothing of rainfall data would likely lead to strong similarity in rainfall time-series of neighboring gridboxes and artificial increases in the variance explained by leading EOTs. In this study a mask is applied where any values of the Rx5day index or monthly total rainfall are missing (see white areas on maps in Figure 1) causing small variations in the EOT coverage between months. Generally, areas of central and inland western Australia are masked in this analysis.

Many Rx5day EOTs have extreme rainfall signatures across reasonably large areas of the continent extending hundreds of kilometers from the base point. This would suggest that, at least for maximum consecutive 5-day rainfall, large-scale processes dominate and drive where locally strong convective rainfall occurs. Isolated convective systems are less likely to produce rainfall amounts that would be detected at more than a small number of stations (or any at all in some central parts of Australia) and therefore are less likely to feature in the EOT correlation maps. Tests on EOTs of maximum 1-day rainfall (Rx1day) indicated greater spatial inhomogeneities in “more extreme” extreme rainfall variability.

3.2 Trends in EOT time series

Linear trends were calculated for each of the EOT time series for mean and extreme rainfall. Only one of 48 extreme rainfall EOTs has a significant trend at the 5% level (March EOT2). This is fewer than would be expected by chance (2.4). This lack of significant trends is in agreement with the findings of other studies (e.g. Haylock and Nicholls 2000; Alexander et al. 2007; Gallant et al. 2007) where few areas of Australia are observed to exhibit significant trends in extreme rainfall. Although, Speer (2008) detected significant decreases in extreme annual east coast rainfall during the second half of the twentieth century. This trend may not be detected in our analysis because it could map onto more than one EOT. Also, the trend may be non-significant for our (longer) period of study.

More total rainfall EOT time series have significant increasing trends (six of 48). All of these EOTs are located in either the Northern Territory or Queensland and occur during the warm season. No EOT time series have significant decreasing trends. This is consistent with trends shown on the Bureau of Meteorology website (http://www.bom.gov.au/climate/change/index.shtml#tabs=Climate-change-tracker&tracker=trend-maps) for the 1930-2012 period. Other studies show different trends when different periods are examined or if station data are used (e.g. Gallant et al. 2007).

3.3 Relationships between remote drivers and EOTs

Indices representing three prominent modes of variability (ENSO, IOD, and SAM) were correlated with each EOT time series to examine the roles of the different potential drivers in extreme (and total) rainfall variability for different areas of Australia. Relationships involving total rainfall EOTs are only discussed when they are distinctly different from results based on extreme rainfall. The EOTs and corresponding correlation coefficients are shown for Rx5day and total rainfall in Tables S1 and S2 respectively. Maps of the normalized regression coefficients of 20CR fields were also plotted and a selection of these are shown. Many of these maps show signatures that resemble patterns typically associated with the climate drivers studied.

3.3.1 ENSO

The relationship between ENSO and each EOT was investigated using the SOI and the Niño-3.4 SST index. The SOI has significant positive correlations with ten of the 12 leading Rx5day EOTs (all except January and June). This suggests La Niña (El Niño) events are associated with higher (lower) values of extreme rainfall in northern and eastern Australia in general. The correlations are weakest in winter when ENSO events are usually not yet developed or are already terminated. There are significant positive correlations in some months with lower-order EOTs located in northern and eastern areas of Australia. The Niño-3.4 index correlations largely reflect the relationships between SOI and the EOTs with all significant correlations being negative. Although, the SST signature associated with ENSO is weaker during the autumn and early winter, so relationships between the Niño-3.4 index and EOTs are generally non-significant at this time of year.

The total rainfall EOTs also show strong relationships with ENSO. The SOI and Niño-3.4 index generally have slightly larger correlations with the total rainfall EOTs than the extreme rainfall EOTs, but have a similar seasonal cycle.

The ENSO relationship with many EOTs can be seen in several of the regression fields. Regressing MSLP on to the leading EOTs of December extreme and total rainfall (Figs. 3a,b) produces similar patterns of lower pressure over the maritime continent and higher pressure over the central equatorial Pacific. This reflects the well-known enhanced Walker-like circulation pattern which increases extreme (and total) rainfall amounts over north-eastern areas of Australia in particular. Heavier rainfall totals in these EOT time series are also associated with the typical ENSO SST pattern: warmer SSTs in the western equatorial Pacific and locally to the Australian region, and cooler SSTs in the central and eastern equatorial Pacific (Figs. 3c,d). Wetter-than-average conditions in many extreme and mean rainfall EOTs are associated with La Niña-like SST patterns and warm local SSTs off the coast of north-east Australia. Previous research has pointed to the important role of locally warm SST anomalies around northern Australia in warm season heavy rainfall events (Evans and Boyer-Souchet 2012). Regressing OLR on to the December EOT1 time series of extreme and total rainfall (Figs. 3e,f) also produces recognizable patterns one might relate to the ENSO phenomenon, such as an intensification of the SPCZ near Queensland associated with increased extreme rainfall.

As the position of the western pole of the SPCZ is strongly correlated to the Niño-3.4 index (Vincent et al. 2011), we also discuss here results using the SPCZ index. The SPCZ is related to some extreme rainfall variability in the north and east of Australia. The SPCZ index has few significant correlations with Rx5day EOTs (four of 48). These are negative correlations, implying that increased extreme rainfall occurs when the western pole of the SPCZ is in a southerly position. Some 20CR fields show an SPCZ-like signature being projected onto several EOTs (e.g. Figs. 3e, f). This is particularly well observed when the OLR field is regressed on to warm season EOTs centered in Queensland. The interannual variability of the summer SPCZ signal is tightly related to the ENSO phenomenon.

In summary, ENSO is a major driver of extreme (and total) rainfall, particularly in the east of the country and during the austral warm season. We observe shifts in the SPCZ related to ENSO and affecting the northeast of Australia. These findings are in agreement with several other studies (Risbey et al. 2009; King et al. 2013a; Min et al. 2013), but they are reached using different methods.

3.3.2 IOD

The IOD is also related to extreme rainfall variability in Australia. Seven out of 48 Rx5day EOTs are significantly correlated to the DMI (Table S1). Most of these are EOTs for extreme rainfall in late autumn to late spring and located in eastern Australia with negative correlations with the DMI. A similar pattern can be observed with the EOTs of total rainfall. The predominance of winter and spring relationships between the IOD and Australian rainfall EOTs is in agreement with previous studies (e.g. Risbey et al. 2009). Removing the ENSO effect (through partial correlations with Niño-3.4) reduces the number of significant relationships (to five for Rx5day EOTs), but not greatly. This illustrates that the IOD relationships with EOTs are probably not statistical artifacts resulting from the ENSO-EOT relationships (assuming all relationships are linear). Warmer SSTs in the eastern Indian Ocean promote wetter conditions in mainland eastern Australia in spring time particularly. Several significant positive correlations exist between the IOD and late summer extreme rainfall EOTs in inland eastern Australia. Although, these relationships do not extend to total rainfall.

3.3.3 SAM

Four of 48 Rx5day EOTs have significant positive correlations with the SAM index (close to the number that might be expected by chance statistically). Nine total rainfall EOTs are significantly correlated with SAM. The majority are positive correlations, although significant negative correlations are observed with total rainfall EOTs in Tasmania. Most EOTs which are associated with the SAM are located in south-eastern Australia. Several of these EOTs in SE Australia are also associated with higher MSLP over the Tasman Sea and onshore flow over the coastlines of New South Wales and southern Queensland. We find several winter-time SAM-EOT relationships, whereas Maher and Sherwood (2014) showed non-significant relationships between SAM and rainfall at this time of year. EOTs with significant SAM relationships also have strong associations with atmospheric blocking south of Australia and the position and intensity of the subtropical ridge (Tables S2, S4). Cowan et al. (2013) found spring-time relationships between positive SAM and enhanced blocking resulting in increased rainfall in SE Australia. Some extreme rainfall EOT time series with significant positive SAM index correlations also have relationships with ENSO indices and Walker-like circulation patterns.

3.4 Relationships between local drivers and EOTs

Indices representing several local drivers (Blocking, Subtropical ridge, and Tropical Cyclones) were also correlated with each EOT time series. The EOTs and corresponding correlation coefficients are shown in Tables S3 and S4. Maps of the normalized regression coefficients of 20CR fields on to EOTs were also plotted. It is worth noting that these local drivers are not independent of the remote drivers discussed previously.

3.4.1 Blocking

The relationships between blocking and extreme rainfall variability were examined first by correlating each Rx5day EOT with the Blocking Index (BI). Of the 48 Rx5day EOTs, 13 have significant correlations with the BI, 11 of these positive. The majority of significant correlations between the BI and EOTs occur in the cool season.

There are many more significant relationships between blocking and total monthly rainfall than extreme rainfall. Twenty-one of the total rainfall EOTs have statistically significant correlations with the BI. The blocking influence extends throughout the year, but is weakest in autumn. The EOTs in mainland SE Australia have positive correlations with the BI, whereas those in the Northern Territory and Tasmania have negative correlations where significant. Risbey et al. (2013) found enhanced blocking is related to an increase in cut-off low systems affecting southeast Australia bringing rainfall to this region.

Signatures of blocking are seen in some of the atmospheric fields from the 20CR. As would be expected, higher values of the BI coincide with EOTs that are associated with increased MSLP south of Australia. Enhanced blocking is related to increased cloudiness in SE Australia, particularly as seen through fields of the OLR regressed on to EOTs. Onshore moist flow along the coast of SE Australia is a feature of EOTs where blocking increases extreme rainfall amounts.

The blocking index (Pook and Gibson 1999) used here is calculated using winds over the 140^{o}E meridian whilst the center of blocking is more commonly further east over the Tasman Sea. Using a different blocking index centered further east would likely lead to fewer significant correlations with EOTs in the Northern Territory and have little effect on results in eastern Australia. Cowan et al. (2013) found blocking at different meridians (130^{o}E and 140^{o}E) had slightly different associations with precipitation patterns. Klingaman et al. (2013) found small differences in the relationships between Queensland seasonal rainfall EOTs and blocking at different longitudes between 120 ^{o}E -180^{o}E.

3.4.2 Subtropical ridge

Six Rx5day EOTs have significant negative correlations with the STR-P index (Fig. 4). When the STR is in an anomalously poleward position there is an associated increase in extreme rainfall in New South Wales and Queensland. The position of the ridge is most strongly related to Eastern Australia extreme rainfall variability from late winter to early summer. The trajectories of rain-bearing systems are influenced by the position of the STR.

The STR position is more strongly related to mean rainfall variability than extreme rainfall variability. Six EOTs of total rainfall have significant positive correlations with STR-P, located in Tasmania, Victoria and southern New South Wales (Fig. 4). Six EOTs centered further north have significant negative correlations with STR-P.

The position of the STR (or the associated subtropical jet) has previously been related to the IPO, SAM, and blocking (e.g. Speer 2008; Kidston et al. 2009; Maher and Sherwood 2014) illustrating the complex nature of investigating the drivers of rainfall patterns in the Australian region. Whilst, the ridge position has strong correlations with rainfall in eastern Australia, these correlations may be the result of covariability with other climate drivers.

The STR-I index also has significant relationships with EOTs (seven for Rx5day and 11 for total rainfall). The intensity index is, in general, negatively correlated with the EOT time series. Thus, a weaker ridge is associated with increased (extreme) rainfall for sites primarily in eastern Australia.

3.4.3 Tropical Cyclones

The monthly TC-E and TC-W indices (see Data and Methods) were calculated for boxes to the north-east and north-west of Australia respectively (Figs. 5a,b). Each TC index is rank correlated with November-April monthly EOTs of extreme and total rainfall. Seven of 24 Rx5day EOTs are significantly positively correlated to the TC-W index, indicating that an increased frequency of TCs passing through the box is related to increased extreme rainfall; six of these EOTs are located in northern Western Australia or the Northern Territory. The leading EOT in December, centered in eastern Queensland, has a significant positive correlation with TC-W, but also with TC-E. There are only two significant correlations between TC-E and the Rx5day EOTs, both of which are positive and located in the east of Queensland.

Eight of 24 mean rainfall EOTs have significant correlations with TC-W. These are mostly positive correlations and for EOTs located in Western Australia and the Northern Territory. There are five significant correlations between TC-E and total rainfall EOTs, four of which are positive and for EOTs in Queensland. Klingaman et al. (2013) also found significant relationships between Coral Sea tropical cyclones and summer rainfall in northern Queensland. Our results contrast somewhat with Lavender and Abbs (2013) who found that closed-low systems (including tropical cyclones) contributed more to extreme rainfall totals than total rainfall.

3.4.4 East Coast Lows

The relationships between east coast lows (ECLs) and extreme rainfall variability were studied through the use of 20CR fields, i.e. without the formation of an index to describe their frequency, locations or intensities. Several EOTs during the cool season have base points on the coast of New South Wales, with strong correlation patterns to the east of the Great Dividing Range extending along the coast of SE Australia. Figure 6a shows the EOT correlation map for August Rx5day EOT3 as an example. ECLs have similar rainfall signatures, with the heaviest precipitation occurring along the coastal fringe. Some general patterns emerge in the atmospheric circulation associated with these EOTs. Increased cloud cover over the immediate area around the location of the EOT and extending into the Tasman Sea to the east can be observed in the OLR fields (Fig. 6b). There are also clearer skies to the south and often positive correlations with the blocking index. These EOTs are generally linked with anomalously high moisture availability over the Tasman Sea and south-west Pacific and anomalous cyclonic circulation (Fig. 6c), patterns that would be associated with east coast lows.

3.5 Predictability of extreme rainfall

Whilst it is useful to advance our understanding of the drivers of extreme rainfall events, it is perhaps of greater importance to improve predictability of these events. Potential sources of prediction skill for above-average monthly extreme (and total) rainfall were investigated. SSTs were regressed on to EOT time series with varying lead times. Several warm season

EOTs of both extreme and total rainfall, such as December extreme rainfall EOT1, have concurrent patterns of regression coefficients with strong ENSO signatures in the Pacific Ocean (Fig. 7l). Regressing SSTs from previous months on to December EOT1, thus introducing a lag, shows predictability from the equatorial Pacific decreasing as the lag increases (Fig. 7). Extending the lag to months prior to the “predictability barrier” of April-June (e.g. Webster and Hoyos 2010) causes the SST signature in the Pacific to largely disappear. However, a potential source of predictability is observed in the Indian Ocean using SST fields from January-March (i.e. 9-11 months in advance). Basin-wide warming in the Indian Ocean during one warm season is related to above-average rainfall in parts of Queensland the following warm season. Averaging January SSTs over the box in Fig. 7a and correlating with December extreme rainfall EOT1 (11 months later) gives a correlation coefficient of 0.27 (0.30 for total rainfall). Scatter plots of January Indian Ocean SSTs and December extreme and total rainfall EOT1 (Figs. 8a,b) show large spread in the relationship, but a clear tendency for a warmer Indian Ocean in January to relate to greater extreme and total rainfall in December. The lagged response of northern Australian rainfall to Indian Ocean warming was previously observed by Taschetto et al. (2011) and may be related to the IOD influence on ENSO more than 12 months in advance (Izumo et al. 2010). Here it is shown that the leading patterns of variability in extreme rainfall in Australia in December have a source of predictability arising from basin-wide Indian Ocean warming from the previous warm season.

Equatorial Pacific Ocean SSTs are related to December extreme and total rainfall at shorter lead times. Scatter plots of September Niño-3.4 region SSTs and December extreme and total rainfall EOT1 (Figs. 8c,d) point to potential predictability of high extreme and total rainfall amounts related to emerging La Niña conditions at a lead time of three months. SST anomalies in the Niño-3.4 region are significantly correlated even a few months apart and this is likely to be behind the predictability at three months lead time (e.g. Jourdain et al. 2013). These potential predictability sources may aid in the forecasting of heavy summer rainfall in Queensland. Although, noise in SST relationships with rainfall points to limits in the predictability of monthly extreme and total rainfall.

There is an asymmetry in the ENSO relationship with warm-season extreme and total rainfall (King et al. 2013a; Cai et al. 2010; Power et al. 2006). This is reflected in concurrent SST regressions onto December extreme rainfall EOT1 for wetter than average and drier than average December Rx5day values separately (Figs. 9l and 10l). There is greater potential for predictability of very wet extremes in Decembers from Pacific SSTs (Fig. 9) than there is of very dry December extremes (Fig. 10). This has important implications for the seasonal forecasting of flood and drought events. There is less of a non-linearity in the relationship between December extreme rainfall EOT1 and Indian Ocean SSTs from the previous warm season (Figs. 9 and 10). These results also extend to mean rainfall (Figs. S5 and S6).

There is lower potential for predictability of January and February leading EOTs of extreme and total rainfall as SST relationships with these time series are weaker (not shown). This is likely related to their locations tending to be further west and in more inland areas (Figure S2).

For some warm season extreme rainfall patterns, particularly in December, there are sources of potential prediction skill arising from Pacific Ocean SSTs a few months in advance and Indian Ocean SSTs up to a year ahead. This potential for predictability extends to total rainfall patterns and could aid in the forecasting of heavy rainfall in north-eastern Australia. In general, however, strong predictability of extreme and total rainfall is not observed and there is high noise in lagged SST relationships with EOTs.

4. Discussion and Conclusions

This study presents an application of an EOT decomposition method to Australian extreme (and mean) rainfall for the investigation of climate drivers and their relative roles in the continent's climate. Use of this method sheds new light on extreme rainfall patterns, their drivers, and the predictability of extreme events.

A number of features are striking from examining the EOTs and their various relationships. The locations of extreme rainfall EOTs differ from those of mean rainfall in the cool season considerably more than in the warm season. The leading EOTs of extreme rainfall tend to be located further north during austral winter than the EOTs of mean rainfall. This reflects the differences in weather systems affecting Australia between the warm and cool seasons. During the winter, mid-latitude synoptic-scale systems pass across southern Australia bringing frontal rainfall over a large area. This has a strong effect on the spatial distribution of total rainfall. However, these frontal systems have less impact on the extreme rainfall index and result in small Rx5day values in many areas of southern Australia.

The predominance of ENSO as a driver of warm-season extreme rainfall variability in eastern Australia is clear, both from EOT relationships with the SOI and Niño-3.4 index, and through examining fields from the 20CR. The SAM and IOD both have weaker roles. Blocking and the subtropical ridge strongly influence total rainfall, particularly during the cool season in southern and eastern Australia. Relationships with extreme rainfall tend to be weaker due to the locations of the Rx5day EOTs being further north.

Several of the extreme rainfall EOTs are strongly related to local weather systems. Tropical cyclones affect warm season EOTs in the north of the continent and east coast lows influence cool season EOTs in the south-east. The EOTs that exhibit east coast low-like patterns have consistent atmospheric features: often an anomalous anticyclone to the south and associated onshore moist flow along the coastal fringe.

Warm-season EOTs are more closely related to SSTs than EOTs during the cool season. The SST fields associated with the leading December EOTs during the austral summer have ENSO-like SST patterns in the Pacific. Potential sources of prediction skill have been identified for above-average monthly rainfall and extreme rainfall through Pacific Ocean SSTs several months in advance and, also Indian Ocean basin-wide warming up to a year ahead. The Pacific conditions provide more information on how much wetter than average conditions could be than on how much drier than average they might be. On the other hand, the relationship between Indian Ocean SSTs and rainfall up to a year later is more linear.

In summary, this study uses a statistical decomposition of rainfall fields to show that extreme rainfall variability in Australia can be related to remote and local drivers as well as large-scale weather systems. The drivers of extreme rainfall variability are more similar to drivers of total rainfall in the warm season than the cool season. Extratropical climate drivers, such as blocking and the subtropical ridge, have weaker relationships with extreme rainfall than mean rainfall. There are potential sources of prediction skill for the most prominent modes of warm season extreme rainfall variability arising from the Pacific and Indian Oceans as much as a year in advance.

Acknowledgments

We thank the editor for handling our submission and we thank Milton Speer and two anonymous reviewers for their helpful and constructive comments which have improved this manuscript. Andrew King and Lisa Alexander were supported by Australian Research Council grant CE110001028. Markus Donat was supported by Australian Research Council grant LP100200690. Nicolas Jourdain was funded by Australian Research Council grant DP110100601. Nicholas Klingaman was funded by the U.K. National Centre for Atmospheric Science, a Natural Environment Research Council collaborative centre, under contract R8/H12/83/001. We thank the Bureau of Meteorology, the Bureau of Rural Sciences, and CSIRO for providing the Australian Water Availability Project data. 20th Century Reanalysis V2 data were provided by the NOAA/OAR/ESRL PSD, Boulder, Colorado, USA, from their website at http://www.esrl.noaa.gov/psd/. Support for the Twentieth Century Reanalysis Project dataset is provided by the U.S. Department of Energy, Office of Science Innovative and Novel Computational Impact on Theory and Experiment (DOE INCITE) program, and Office of Biological and Environmental Research (BER), and by the National Oceanic and Atmospheric Administration Climate Program Office. HadISST SSTs were provided by the U.K. Met Office. IBTrACS data were provided by the U.S. National Climatic Data Center.

References

Alexander, L. V., P. Hope, D. Collins, B. Trewin, A. Lynch, and N. Nicholls,. 2007: Trends in Australia's climate mean and extremes: a global context. *Aust. Met. Mag.,* **56**, 1-18.

Allan, R., 1988: El Niño-Southern Oscillation influences in the Australasian region. *Prog. in Phys. Geog.,* **12**, 313-348.

Ashcroft, L., D. J. Karoly, and J. Gergis, 2013: Southeastern Australian climate variability 1860-2009: a multivariate analysis. *Int. J. Climatol.,* doi: 10.1002/joc.3812.

Brown, J. R., S. B. Power, F. P. Delage, R. A. Colman, A. F. Moise, and B. F. Murphy, 2011: Evaluation of the South Pacific Convergence Zone in IPCC AR4 Climate Model Simulations of the Twentieth Century. *J. Climate*, **24**, 1565-1582, doi: 10.1175/2010JCLI3942.1.

Cai, W., and T. Cowan, 2006: SAM and regional rainfall in IPCC AR4 models: Can anthropogenic forcing account for southwest Western Australian winter rainfall reduction? *Geophys. Res. Lett.,* **33**, L24708, doi:10.1029/2006GL028037.

Cai, W., P. van Rensch, and T. Cowan, 2011: Influence of Global-Scale Variability on the Subtropical Ridge over Southeast Australia. *J. Climate*, **24**, 6035-6053.

Cai, W., P. van Rensch, T. Cowan, and A. Sullivan, 2010: Asymmetry in ENSO Teleconnection with Regional Rainfall, Its Multidecadal Variability and Impact. *J. Climate,* **23**, 4944-4955.

Cai, W., P. H. Whetton, and A. B. Pittock, 2001: Fluctuations of the relationship between ENSO and northeast Australian rainfall. *Clim. Dyn.,* **17**, 421-432.

Compo, G. P., and Coauthors, 2011: The twentieth century reanalysis project. *Q. J. Roy. Meteorol. Soc.,* **137**, 1-28, doi: 10.1002/qj.776.

Cowan, T., P. van Rensch, A. Purich, and W. Cai, 2013: The Association of Tropical and Extratropical Climate Modes to Atmospheric Blocking across Southeastern Australia. *J. Climate,* **26**, 7555-7569, doi: 10.1175/JCLI-D-12-00781.1.

Donat, M. G., L. V. Alexander, H. Yang, I. Durre, R. Vose, and J. Caesar, 2013: Global Land-Based Datasets for Monitoring Climatic Extremes. *Bull. Amer. Meteor. Soc.,* **94**, 997-1006, doi:10.1175/BAMS-D-12-00109.1.

Evans, J. P., and I. Boyer-Souchet, 2012: Local sea surface temperatures add to extreme precipitation in northeast Australia during La Niña. *Geophys. Res. Lett.,* **39**, L10803, doi:10.1029/2012GL052014.

Feng, J., J. Li, and Y. Li, 2010: Is There a Relationship between the SAM and Southwest Western Australian Winter Rainfall? *J. Climate,* **23**, 6082-6089.

Gallant, A. J. E., K. J. Hennessy, and J. Risbey, 2007: Trends in rainfall indices for six Australian regions: 1910-2005. *Aust. Met. Mag.,* **56**, 223-239.

Gallant, A. J. E., A. S. Kiem, D. C. Verdon-Kidd, R. C. Stone, and D. J. Karoly, 2012: Understanding hydroclimate processes in the Murray-Darling Basin for natural resources management. *Hydrol. Earth Syst. Sci.,* **16**, 2049-2068, doi: 10.5194/hess-16-2049-2012.

Gong, D, and S. Wang, 1999: Definition of Antarctic Oscillation Index. *Geophys. Res. Letts.,* **26**, 459-462.

Haylock, M., and N. Nicholls, 2000: Trends in extreme rainfall indices for an updated high quality dataset for Australia, 1910-1998. *Int. J. Climatol.,* **20**, 1533-1541.

Hendon, H. H., E.-P. Lim, J. M. Arblaster, and D. L. T. Anderson, 2014: Causes and predictability of the record wet east Australian spring 2010. *Clim. Dyn.*, **42**, 1155-1174, doi: 10.1007/s00382-013-1700-5.

Holland, G. J., 1986: Interannual Variability of the Australian Summer Monsoon at Darwin: 1952-82. *Mon. Wea. Rev.,* **114**, 594-604.

Izumo, T., and Coauthors, 2010: Influence of the state of the Indian Ocean Dipole on the following year's El Niño. *Nat. Geosci.,* **3**, 168-172.

Jones D. A., W. Wang, and R. Fawcett, 2009: High-quality spatial climate data-sets for Australia. *Aust. Meteor. Ocean. J.,* **58**, 233-248.

Jourdain, N. C., A. S. Gupta, A. S., Taschetto, C. C. Ummenhofer, A. F. Moise, and K. Ashok, 2013: The Indo-Australian monsoon and its relationship to ENSO and IOD in reanalysis data and the CMIP3/CMIP5 simulations. *Clim. Dyn.*, **41**, 3073-3102.

Kidston, J., J. A. Renwick, and J. McGregor, 2009: Hemispheric-Scale Seasonality of the Southern Annular Mode and Impacts on the Climate of New Zealand. *J. Climate,* **22**, 4759-4770, doi: 10.1175/2009JCLI2640.1

King, A. D., L. V. Alexander, and M. G. Donat, 2013a: Asymmetry in the response of Eastern Australia extreme rainfall to low-frequency Pacific variability. *Geophys. Res. Lett.*, **40**, 2271-2277, doi: 10.1002/grl.50427.

King, A. D., L. V. Alexander, and M. G. Donat, 2013b: The efficacy of using gridded data to examine extreme rainfall characteristics: A case study for Australia. *Int. J. Climatol.*, **33**, 2376-2387. doi: 10.1002/joc.3588.

King, A. D., S. C. Lewis, S. E. Perkins, L. V. Alexander, M. G. Donat, D. J. Karoly, and M. T. Black, 2013c: Limited Evidence of Anthropogenic Influence on the 2011-12 Extreme Rainfall over Southeast Australia [in "Explaining Extreme Events of 2012 from a Climate Perspective"], *Bull. Amer. Meteor. Soc.*, **94** (9), S55-S58.

Klingaman, N. P., S. J. Woolnough, and J. Syktus, 2013: On the drivers of inter-annual and decadal rainfall variability in Queensland, Australia, *Int. J. Climatol.*, **33**, 2413-2430. doi: 10.1002/joc.3593.

Knapp, K. R., M. C. Kruk, D. H. Levinson, H. J. Diamond, and C. J. Neumann, 2010: The international best track archive for climate stewardship (IBTrACS). *Bull. Amer. Met. Soc.*, **91**, 363-376.

Larsen, S. H., and N. Nicholls, 2009: Southern Australian rainfall and the subtropical ridge: Variations, Interrelationships, and trends. *Geophys. Res. Lett.*, **36**, L08708, doi:10.1029/2009GL037786.

Lavender, S. L., and D. J. Abbs, 2013: Trends in Australian rainfall: contribution of tropical cyclones and closed lows. *Clim. Dyn.*, doi:10.1007/s00382-012-1566-y.

Madden, R. A., and P. Julian, 1971: Detection of a 40-50 day oscillation in the zonal wind. *J. Atmos. Sci.*, **28**, 702-708.

Maher, P. and S. C. Sherwood, 2014: Disentangling the multiple sources of large-scale variability in Australian wintertime precipitation. *J. Climate*, accepted.

Marshall, G., 2003: Trends in the southern annular mode from observations and reanalyses. *J. Climate,* **16**, 4134-4143.

McBride, J. L., and N. Nicholls, 1983: Seasonal Relationships between Australian Rainfall and the Southern Oscillation. *Mon. Wea. Rev.*, **111**, 1998-2004.

Meneghini, B., I. Simmonds, and I. N. Smith, 2007: Association between Australian rainfall and the southern annular mode. *Int. J. Climatol.*, **27**, 109-121.

Meyers, G., P. McIntosh, L. Pigot, and M. Pook, 2007: The years of El Niño, La Niña and interactions with the tropical Indian Ocean. *J. Climate,* **20**, 2872–2880, doi:10.1175/JCLI4152.1.

Min, S.-K., W. Cai, and P. Whetton, 2012: Influence of climate variability on seasonal extremes over Australia. *J. Geophys. Res. Atmos.*, **118**, 643-654, doi:10.1002/jgrd.50164.

Nicholls, N., W. Drosdowsky, and B. Lavery, 1997: Australian rainfall variability and change. *Weather*, **52**, 66-71.

Nicholls, N., B. Lavery, C. Frederiksen, W. Drosdowsky, and S. Torok, 1996: Recent apparent changes in relationships between the El Niño-southern oscillation and Australian rainfall and temperature. *Geophys. Res. Lett.*, **23**, 3357-3360.

Parker, D., C. Folland, A. Scaife, J. Knight, A. Colman, P. Baines, and B. Dong, 2007: Decadal to multidecadal variability and the climate change background. *J. Geophys. Res.*, **112**, D18115, doi:10.1029/2007JD008411.

Pook, M., and T. Gibson, 1999: Atmospheric blocking and storm tracks during SOP-1 of the FROST project. *Aust. Met. Mag.*,**Spec. Ed.,** 51-60.

Power, S., M. Haylock, R. Colman, and X. Wang, 2006: The Predictability of Interdecadal Changes in ENSO Activity and ENSO Teleconnections. *J. Climate*, **19**, 4755-4771.

Rayner, N. A., P. Brohan, D. E. Parker, C. K. Folland, J. J. Kennedy, M. Vanicek, T. Ansell, and S. F. B. Tett, 2006: Improved analyses of changes and uncertainties in sea surface temperature measured in situ since the mid-nineteenth century: the HadSST2 data set. *J. Climate,* **19**, 446-469.

Rayner, N. A., D. E. Parker, E. B. Horton, C. K. Folland, L. V. Alexander, D. P. Rowell, E. C. Kent, and A. Kaplan, 2003: Global analyses of sea surface temperature, sea ice, and night marine air temperature since the late nineteenth century. *J. Geophys. Res.*, **108**, D14, 4407, doi:10.1029/2002JD002670.

Risbey, J. S., P. C. McIntosh, and M. J. Pook, 2013: Synoptic components of rainfall variability and trends in southeast Australia. *Int. J. Climatol.*, **33**, 2459–2472, doi: 10.1002/joc.3597.

Risbey, J. S., M. J. Pook, P. C. McIntosh, M. C. Wheeler, and H. H. Hendon, 2009: On the Remote Drivers of Rainfall Variability in Australia. *Mon. Wea. Rev.* **137**, 3233-3253.

Rotstayn, L. D., M. A. Collier, M. R. Dix, Y. Feng, H. B. Gordon, S. P. O'Farrell, I. N. Smith, and J. Syktus, 2010: Improved simulation of Australian climate and ENSO-related rainfall variability in a global climate model with an interactive aerosol treatment. *Int. J. Climatol.,* **30**, 1067-1088.

Saji, N. H., B. N. Goswami, P. N. Vinayachandran, and T. Yamagata, 1999: A dipole mode in the tropical Indian Ocean. *Nature,* **401**, 360-363.

Smith, I., 2004: An assessment of recent trends in Australian rainfall. *Aust. Met. Mag.*, **53**, 163-173.

Speer, M. S., 2008: On the late twentieth century decrease in Australian east coast rainfall extremes. *Atmos. Sci. Lett.*, **9**, 160-170, doi: 10.1002/asl.191.

Speer, M. S., L. M. Leslie, and A. O. Fierro, 2011: Australian east coast rainfall decline related to large scale climate drivers. *Clim. Dyn.*, **36**, 1419-1429, doi: 10.1007/s00382-009-0726-1.

Taschetto, A. S., A. Sen Gupta, H. H. Hendon, C. C. Ummenhofer, and M. H. England, 2011: The Contribution of Indian Ocean Sea Surface Temperature Anomalies on Australian Summer Rainfall during El Niño Events. *J. Climate*, **24**, 3734-3747.

Timbal, B. and W. Drosdowsky, 2013: The relationship between the decline of Southeastern Australian rainfall and the strengthening of the subtropical ridge. *Int. J. Climatol.*, **33**, 1021-1034, doi:10.1002/joc.3492.

Trenberth, K., 1984: Signal versus Noise in the Southern Oscillation. *Mon. Wea. Rev.*, **112,** 326-332.

Ummenhofer, C. C., M. H. England, P. C. McIntosh, G. A. Meyers, M. J. Pook, J. S. Risbey, A. S. Gupta, and A. S. Taschetto, 2009: What causes southeast Australia's worst droughts? *Geophys. Res. Lett.*, **36**, L04706, doi:10.1029/2008GL036801.

Ummenhofer, C. C., A. S. Gupta, P. R. Briggs, M. H. England, P. C. McIntosh, G. A. Meyers, M. J. Pook, M. R. Raupach, and J. S. Risbey, 2011: Indian and Pacific Ocean influences on Southeast Australian drought and soil moisture. *J. Climate*, **24**, 1313–1336, doi:10.1175/2010JCLI3475.1.

van den Dool H. M., S. Saha, and A. Johansson, 2000: Empirical Orthogonal Teleconnections. *J. Climate*, **13**, 1421-1435.

Vincent, E. M., M. Lengaigne, C. E. Menkes, N. C. Jourdain, P. Marchesiello, and G. Madec, 2011: Interannual variability of the South Pacific Convergence Zone and implications for tropical cyclone genesis. *Clim. Dyn.*, **36**, 1881-1896. doi:10.1007/s00382-009-0716-3.

Webster, P. J., and C. D. Hoyos, 2010: Beyond the spring barrier? *Nat. Geosci.*, **3**, 152-153.

Whan, K., B. Timbal, and J. Lindesay, 2013: Linear and nonlinear statistical analysis of the impact of sub-tropical ridge intensity and position on south-east Australian rainfall. *Int. J. Climatol.*, in press, doi:10.1002/joc.3689.

Zhang, X, L. Alexander, G. C. Hegerl, P. Jones, A. K. Tank, T. C. Peterson, B. Trewin, and F. W. Zwiers, 2011: Indices for monitoring changes in extremes based on daily temperature and precipitation data. *Wiley Interdiscip. Rev. Clim. Change,* **2**, 851–870, doi: 10.1002/wcc.147.

Figures

Figure 1: Map of Australian states and territories referred to in this study. The abbreviations stand for the following states and territories: NSW- New South Wales, NT- Northern Territory, QLD- Queensland, SA- South Australia, TAS- Tasmania, VIC- Victoria, and WA- Western Australia.

Figure 2: Maps of the locations of leading EOTs (blue triangles) and the correlations between EOT time series (i.e. base-point time series) and time series at all other grid points for (a) January Rx5day, (b) January total rainfall, (c) August Rx5day and (d) August total rainfall. Stippling indicates where the correlations are significant at the 5% level. White areas over Australia indicate masking where there is at least one missing data point in the time series.

Figure 3: Maps of (a), (b) MSLP, (c), (d) SSTs, and (e), (f) OLR regressed on to December EOT1 of Rx5day and total rainfall respectively. Stippling indicates 5% significance in the correlation coefficients.

Figure 4: Map of the locations of significant correlations (at the 5% level) between the sub-tropical ridge position index and EOT time series. Positive and negative correlations are indicated by the upward and downward pointing triangles respectively.

Figure 5: Maps of the locations of Rx5day (blue) and Total rainfall (red) EOTs correlated at the 5% level with the (a) TC-E and (b) TC-W indices. Positive and negative correlations are indicated by the upward and downward pointing triangles respectively. The boxes in a) and b) represent the areas for which tropical cyclone counts are calculated for TC-E and TC-W indices respectively.

Figure 6: (a) Map of the location of the August Rx5day EOT3 (blue triangle) and the correlations between EOT time series and all other residual time series. Stippling indicates

where the correlations are significant at the 5% level. White areas over Australia indicate masking where there is at least one missing data point in the time series. (b) Map of OLR regressed on to August Rx5day EOT3. Stippling indicates where the correlation coefficients are significant at the 5% level. (c) Map of 850hPa moisture and winds (arrows) regressed on to August Rx5day EOT3.

Figure 7: (a-l) Maps of SSTs from each calendar month from (a) January to (l) December regressed on to December Rx5day EOT1. The boxed region in (a) is used to calculate mean January SSTs in the equatorial Indian Ocean to examine relationships with the EOT. The boxed region in (i) is used to calculate September Niño-3.4 region SSTs. Stippling indicates 5% significance of the correlation between SSTs and the EOT.

Figure 8: (a-b) Scatter plots of January equatorial Indian Ocean SST anomalies versus (a) December Rx5day EOT1 and (b) December Total EOT1. Lines of best fit (black solid) are shown across all SST anomalies with slope, correlation coefficient and p-value. (c-d) Scatter plots of September Niño-3.4 SST anomalies versus (c) December Rx5day EOT1 and (d) December Total EOT1. Lines of best fit (blue and red) are shown for negative and positive SST anomalies respectively with slope, rank correlation coefficient and p-value.

Figure 9: (a-l) Maps of SSTs from each calendar month from (a) January to (l) December regressed on to December Rx5day EOT1 for wetter than average December Rx5day values only. Stippling indicates 5% significance of the correlation between SSTs and the EOT.

Figure 10: (a-l) Maps of SSTs from each calendar month from (a) January to (l) December regressed on to December Rx5day EOT1 for drier than average December Rx5day values only. Stippling indicates 5% significance of the correlation between SSTs and the EOT.

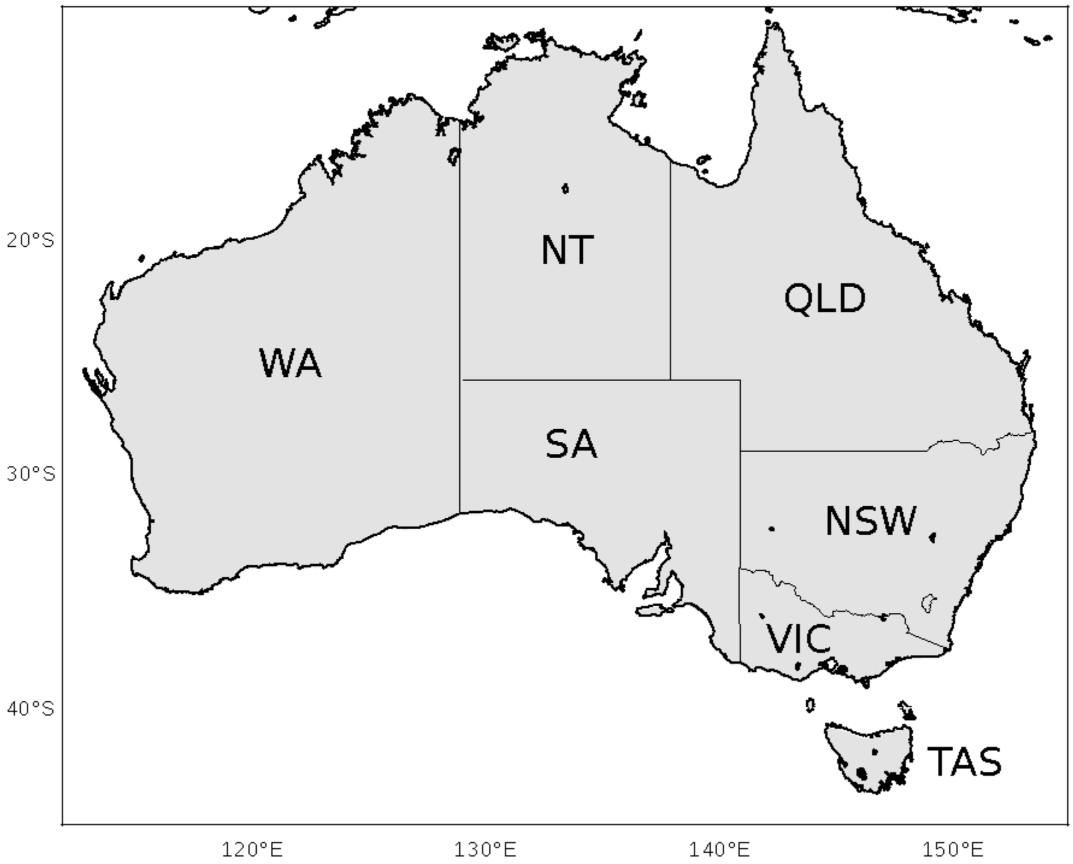

Figure 1: Map of Australian states and territories referred to in this study. The abbreviations stand for the following states and territories: NSW- New South Wales, NT- Northern Territory, QLD- Queensland, SA- South Australia, TAS- Tasmania, VIC- Victoria, and WA- Western Australia.

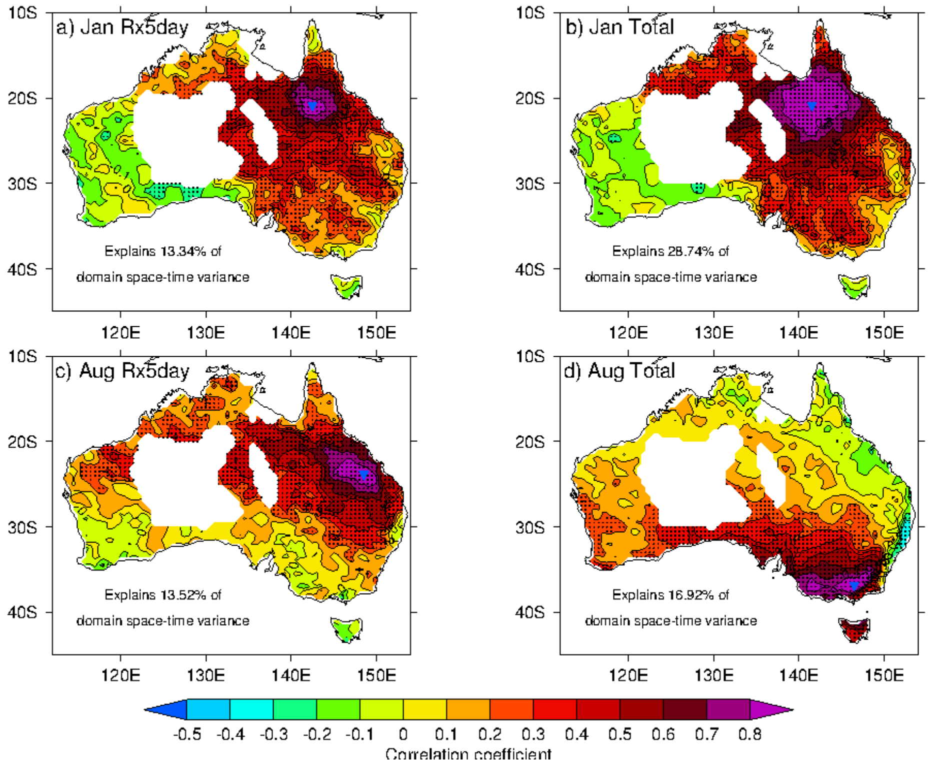

Figure 2: Maps of the locations of leading EOTs (blue triangles) and the correlations between EOT time series (i.e. base-point time series) and time series at all other grid points for (a) January Rx5day, (b) January total rainfall, (c) August Rx5day and (d) August total rainfall. Stippling indicates where the correlations are significant at the 5% level. White areas over Australia indicate masking where there is at least one missing data point in the time series.

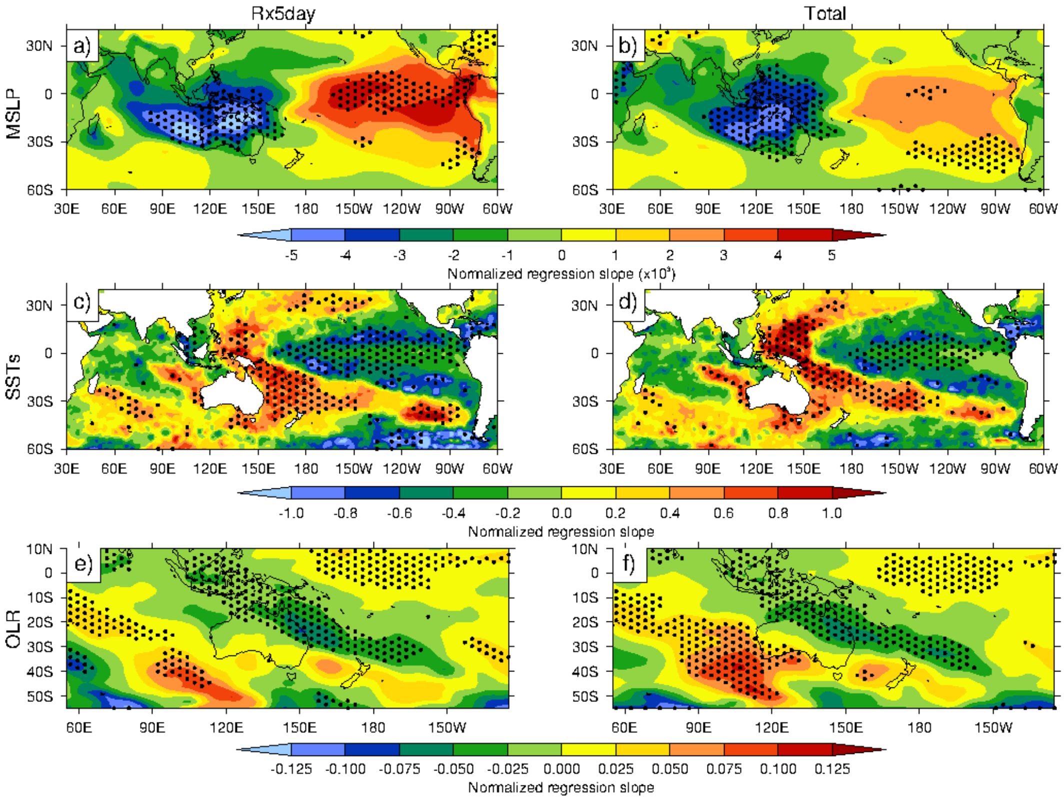

Figure 3: Maps of (a), (b) MSLP, (c), (d) SSTs, and (e), (f) OLR regressed on to December EOT1 of Rx5day and total rainfall respectively. Stippling indicates 5% significance in the correlation coefficients.

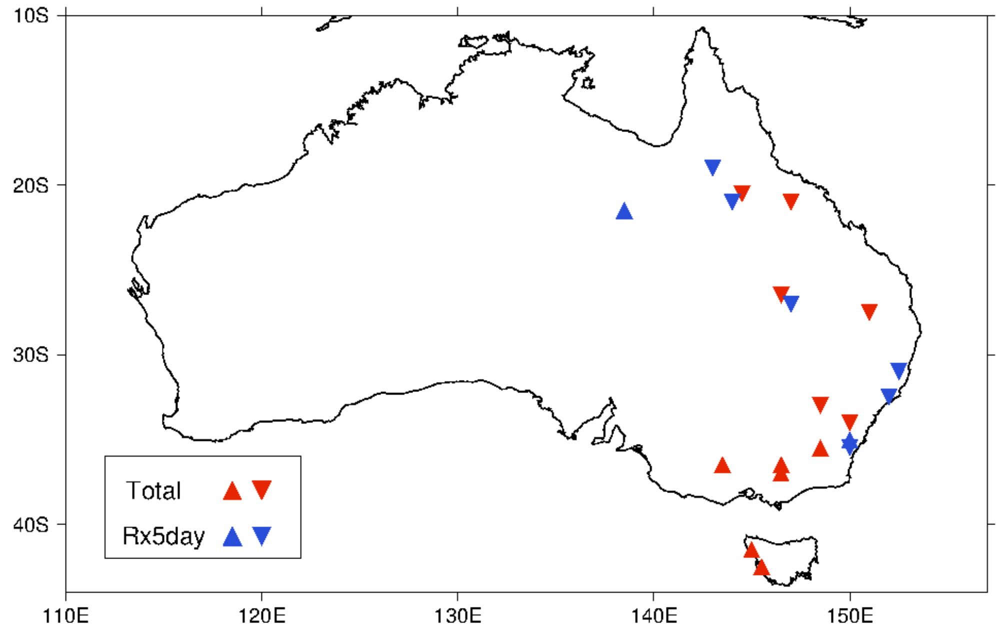

Figure 4: Map of the locations of significant correlations (at the 5% level) between the sub-tropical ridge position index and EOT time series. Positive and negative correlations are indicated by the upward and downward pointing triangles respectively.

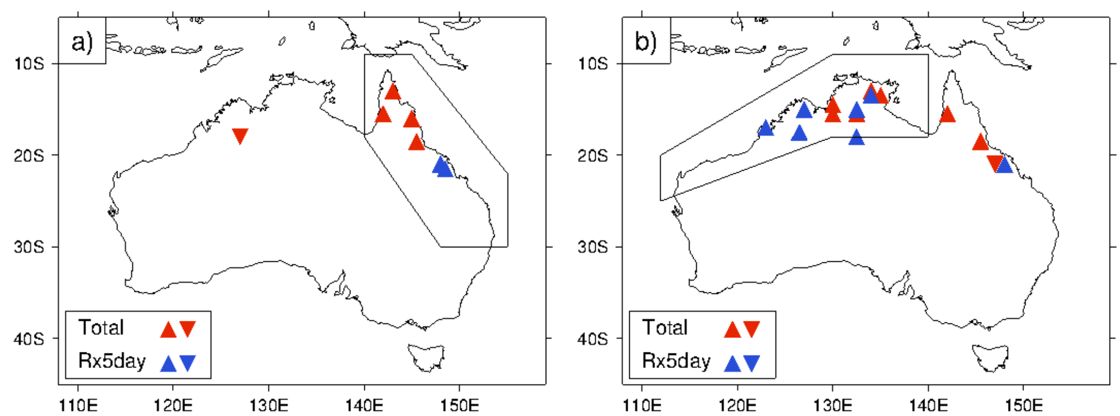

Figure 5: Maps of the locations of Rx5day (blue) and Total rainfall (red) EOTs correlated at the 5% level with the (a) TC-E and (b) TC-W indices. Positive and negative correlations are

indicated by the upward and downward pointing triangles respectively. The boxes in a) and b) represent the areas for which tropical cyclone counts are calculated for TC-E and TC-W indices respectively.

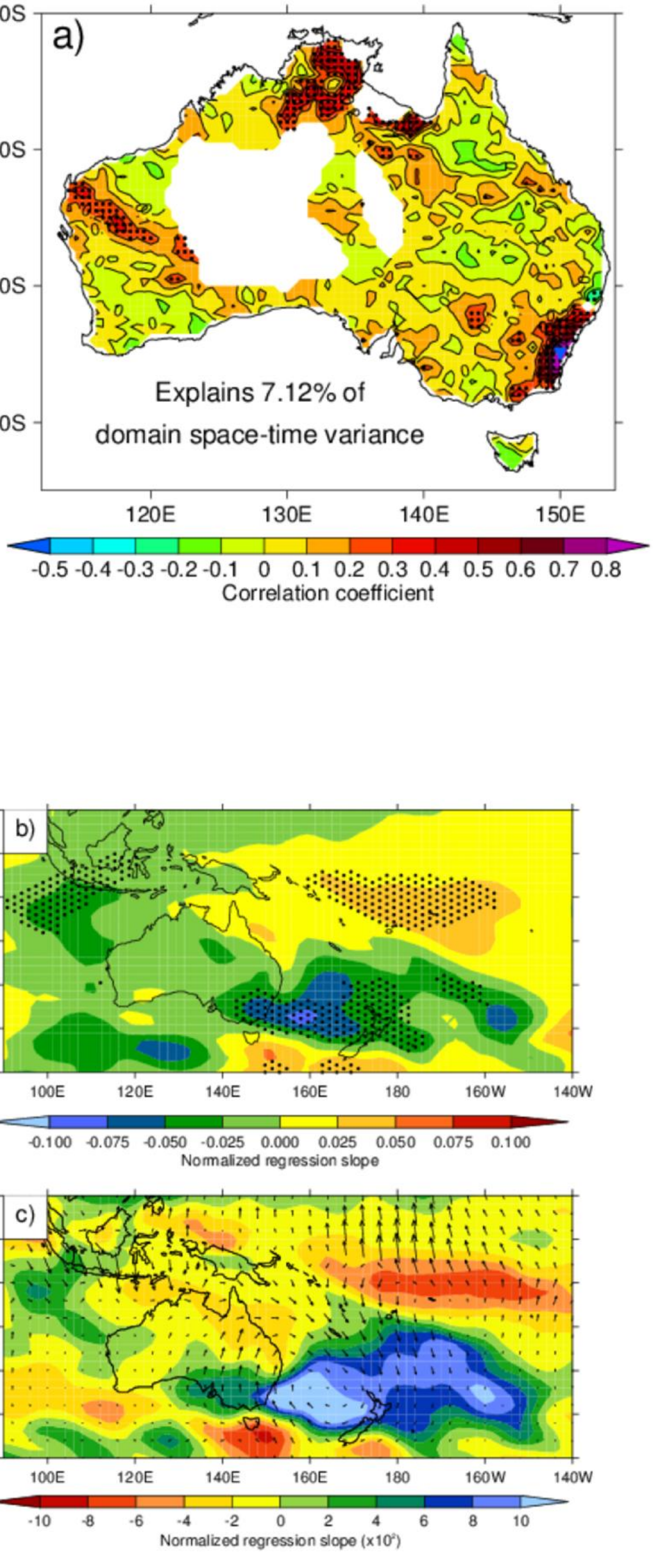
a)
Explains 7.12% of
domain space-time variance
10S
20S
30S
40S
120E 130E 140E 150E
-0.5 -0.4 -0.3 -0.2 -0.1 0 0.1 0.2 0.3 0.4 0.5 0.6 0.7 0.8
Correlation coefficient
b)
10N 0 10S 20S 30S 40S 50S
100E 120E 140E 160E 180 160W 140W
-0.100 -0.075 -0.050 -0.025 0.000 0.025 0.050 0.075 0.100
Normalized regression slope
c)
10N 0 10S 20S 30S 40S 50S
100E 120E 140E 160E 180 160W 140W
-10 -8 -6 -4 -2 0 2 4 6 8 10
Normalized regression slope (x10²)

Figure 6: (a) Map of the location of the August Rx5day EOT3 (blue triangle) and the correlations between EOT time series and all other residual time series. Stippling indicates where the correlations are significant at the 5% level. White areas over Australia indicate masking where there is at least one missing data point in the time series. (b) Map of OLR regressed on to August Rx5day EOT3. Stippling indicates where the correlation coefficients are significant at the 5% level. (c) Map of 850hPa moisture and winds (arrows) regressed on to August Rx5day EOT3.

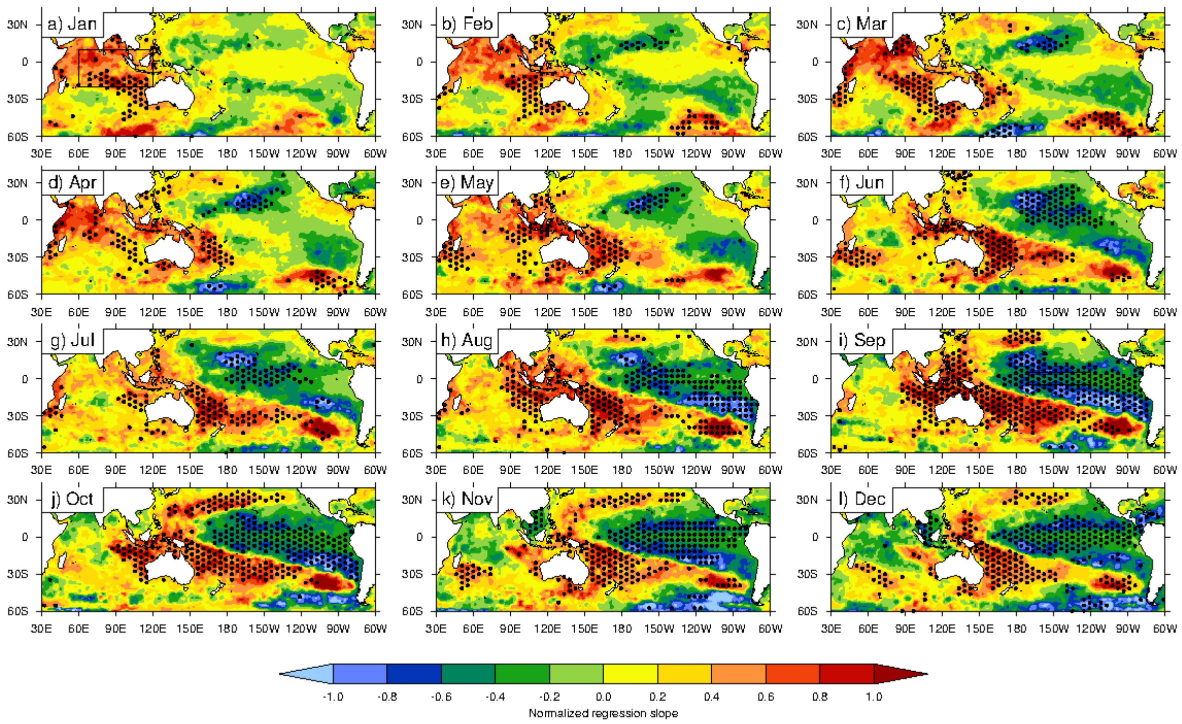

Figure 7: (a-l) Maps of SSTs from each calendar month from (a) January to (l) December regressed on to December Rx5day EOT1. The boxed region in (a) is used to calculate mean January SSTs in the equatorial Indian Ocean to examine relationships with the EOT. The boxed region in (i) is used to calculate September Niño-3.4 region SSTs. Stippling indicates 5% significance of the correlation between SSTs and the EOT.

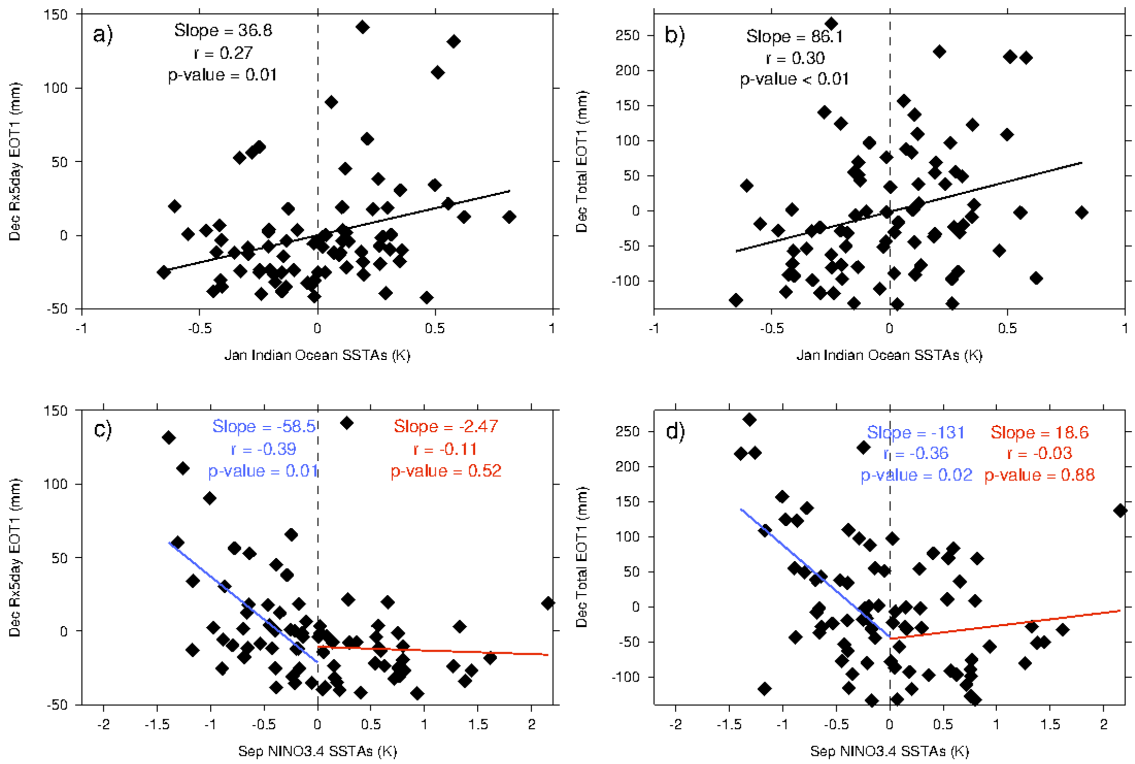

Figure 8: (a-b) Scatter plots of January equatorial Indian Ocean SST anomalies versus (a) December Rx5day EOT1 and (b) December Total EOT1. Lines of best fit (black solid) are shown across all SST anomalies with slope, correlation coefficient and p-value. (c-d) Scatter plots of September Niño-3.4 SST anomalies versus (c) December Rx5day EOT1 and (d) December Total EOT1. Lines of best fit (blue and red) are shown for negative and positive SST anomalies respectively with slope, rank correlation coefficient and p-value.

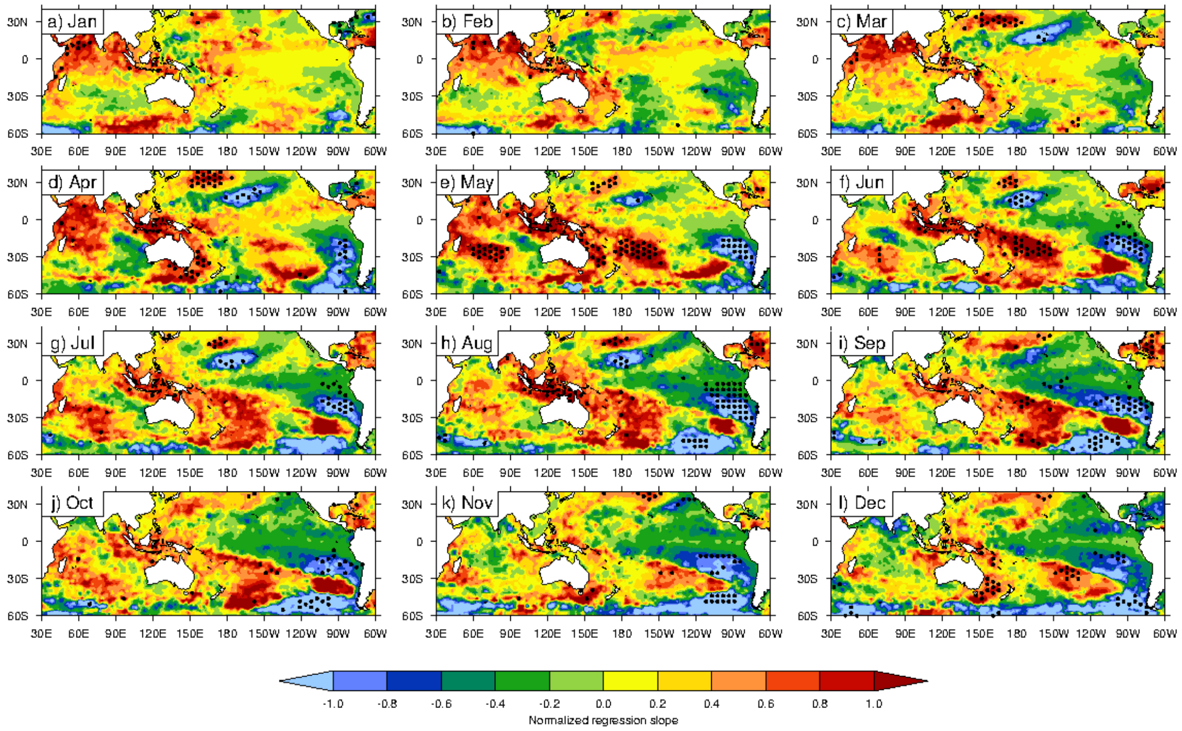

Figure 9: (a-l) Maps of SSTs from each calendar month from (a) January to (l) December regressed on to December Rx5day EOT1 for wetter than average December Rx5day values only. Stippling indicates 5% significance of the correlation between SSTs and the EOT.

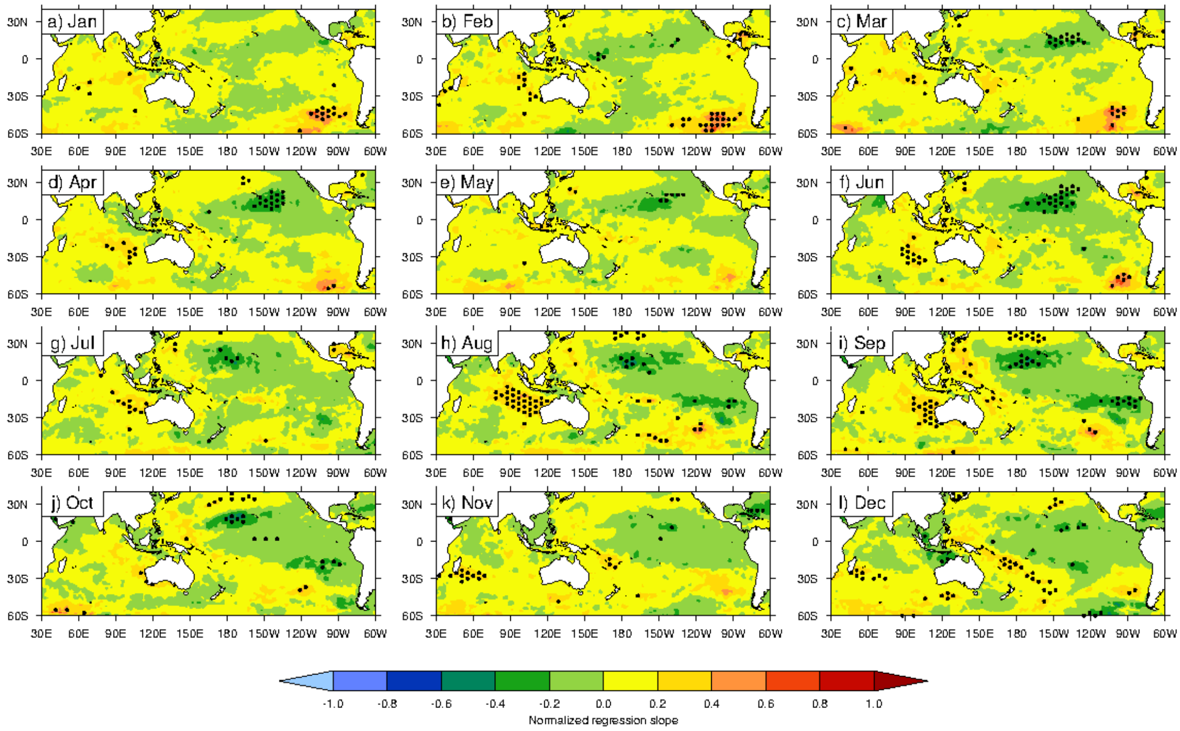

Figure 10: (a-l) Maps of SSTs from each calendar month from (a) January to (l) December regressed on to December Rx5day EOT1 for drier than average December Rx5day values only. Stippling indicates 5% significance of the correlation between SSTs and the EOT.

Supplementary Material

Supplementary Text

The Empirical Orthogonal Teleconnection (EOT) method of statistical decomposition was developed by van den Dool et al. (2000) and bears strong similarities to the more commonly used Empirical Orthogonal Function (EOF) analysis. Unlike EOFs, however, EOTs are only orthogonal in either time or space. In this study the EOTs are orthogonal in time. Therefore, the method employed in this study involves finding the point in space whose time series bears the strongest similarity to the time series at all other points (as measured by the correlation coefficient). The time series at that point (called the base point) is then the leading EOT and its signature is removed from all other time series to create residuals. The same process is then applied to the new residual time series to find the second EOT. This process may continue to find however many EOTs are desired up to a limit equal to the number of gridboxes - in this study we calculate the first four (chosen as a compromise between gaining additional EOTs to study their drivers, and not examining EOTs with very low explained space-time variance). This method was adapted by Smith (2004) for Australia to account for the large spatial gradients in rainfall between coastal and inland areas. Smith (2004) calculated EOTs based on variance in area-average rainfall as opposed to the sum of variance across all points. The Smith (2004) method has since been employed to examine inter-annual rainfall variability over Australia in the CSIRO Mk3.6 model (Rotstayn et al., 2010), and to study interannual-to-multidecadal rainfall variability in Queensland (Klingaman et al., 2013). To the knowledge of the authors this is the first study to apply the Smith (2004) method to look at extreme rainfall as well as total rainfall.

The method of calculating EOTs on a gridded dataset raises a number of potential issues. The gridded dataset has a varying station network in time and space and, given that the EOT method involves comparing time-series of individual gridboxes, several tests were required and steps taken to ensure the robustness of results. Firstly, all data analyzed in this study starts from 1930 at the earliest. Prior to 1930 there is a rapid rise in the number of stations used to generate the AWAP gridded dataset (Jones et al., 2009). Whilst there is still some temporal variability in stations used to form AWAP after 1930, it is substantially reduced from earlier on in the twentieth century. Using different start dates, such as 1907 and 1950 does not have a large effect on the locations of the EOT base points. The EOT method was also applied to precipitation data from the 20CR (Compo et al., 2011) and GHCNDEX (Donat et al., 2013) and found to produce similar patterns.

EOTs of total rainfall and Rx5day were calculated from the 20CR for comparison with the EOTs from AWAP regridded to a 2-degree resolution (to match the resolution of the 20CR). As there is complete data coverage, EOTs in the 20CR could be calculated both with and without a mask. Patterns of leading EOTs in the unmasked 20CR tend to be centered further west during the warmer months and further south in the cool months when compared with the leading EOTs in AWAP. The patterns also spread more into the center and west of Australia, increasing the associated space-time variance. The EOTs in the masked 20CR are in similar locations to those in AWAP. The EOTs centered on the coast of New South Wales during the cool season in the observations are not replicated in the 20CR but this is likely due to the coarser nature of the land-sea mask in the reanalysis.

Supplementary Figures

These supplementary figures are referred to in the main text.

Figure S1: Timeseries of climate indices used in this study: a) Southern Oscillation Index (SOI), b) Niño-3.4 index, c) South Pacific Convergence Zone (SPCZ) index, d) Dipole Mode Index (DMI), e) Southern Annular Mode (SAM) index, f) Blocking Index (BI), g) Subtropical ridge position (STR-P) index, h) Subtropical ridge intensity (STR-I) index, i) Tropical Cyclone West (TC-W) index, and j) Tropical Cyclone East (TC-E) index.

Figure S2: (a-l) The locations of the first four Rx5day (blue numbers) and Total rainfall (red numbers) EOTs for each calendar month from (a) June to (l) May.

Figure S3: Fraction of total variance explained by each of the first four total (red) and Rx5day (blue) EOTs for each calendar month. The size of the diamond decreases for lower-order EOTs (i.e. the largest diamond represents the first EOT).

Figure S4: (a-l) As Figure 7 for December total rainfall EOT1.

Figure S5: (a-l) As Figure 9 for December total rainfall EOT1.

Figure S6: (a-l) As Figure 10 for December total rainfall EOT1.

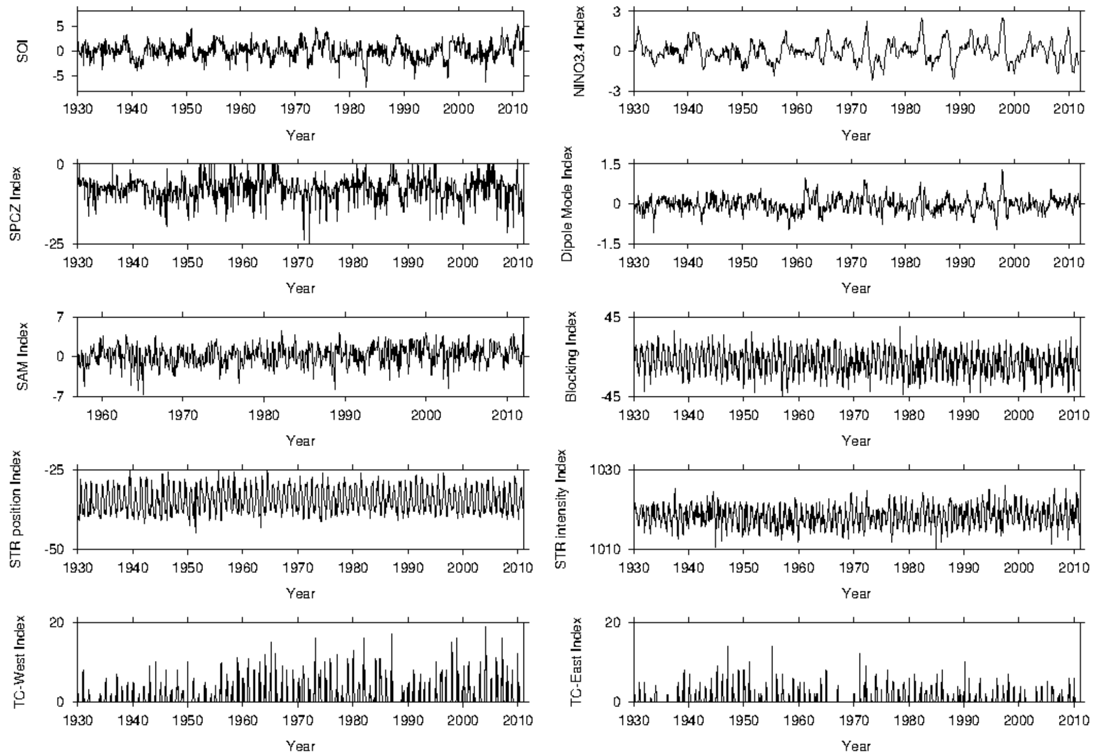

Figure S1: Timeseries of climate indices used in this study: a) Southern Oscillation Index (SOI), b) Niño-3.4 index, c) South Pacific Convergence Zone (SPCZ) index, d) Dipole Mode Index (DMI), e) Southern Annular Mode (SAM) index, f) Blocking Index (BI), g) Subtropical ridge position (STR-P) index, h) Subtropical ridge intensity (STR-I) index, i) Tropical Cyclone West (TC-W) index, and j) Tropical Cyclone East (TC-E) index.

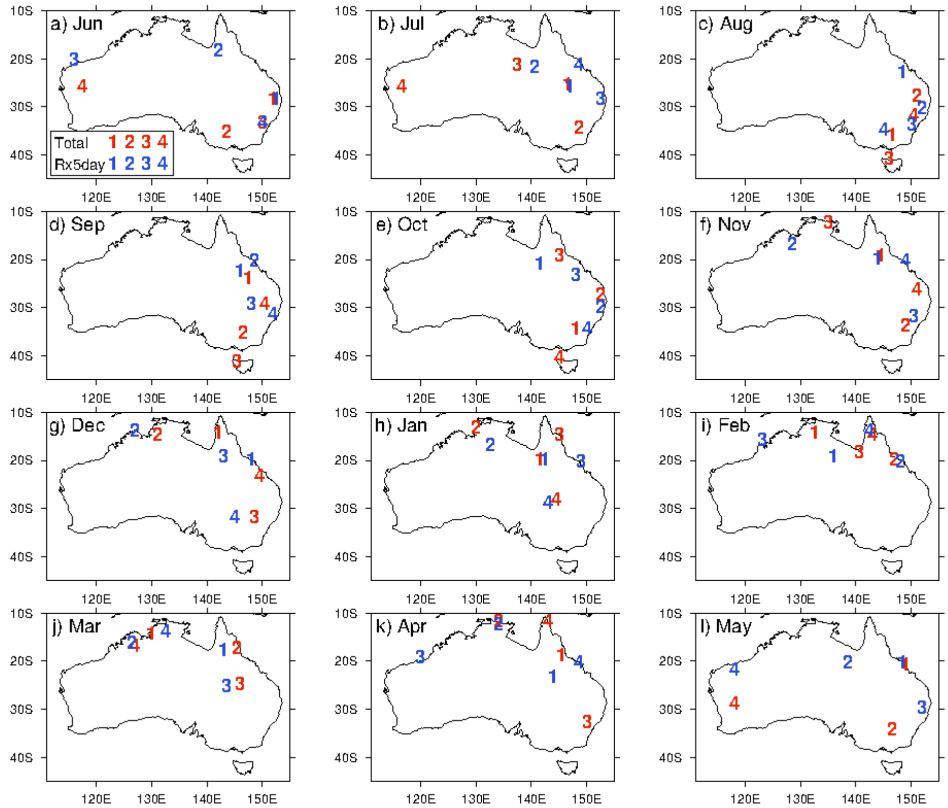

Figure S2: (a-l) The locations of the first four Rx5day (blue numbers) and Total rainfall (red numbers) EOTs for each calendar month from (a) June to (l) May.

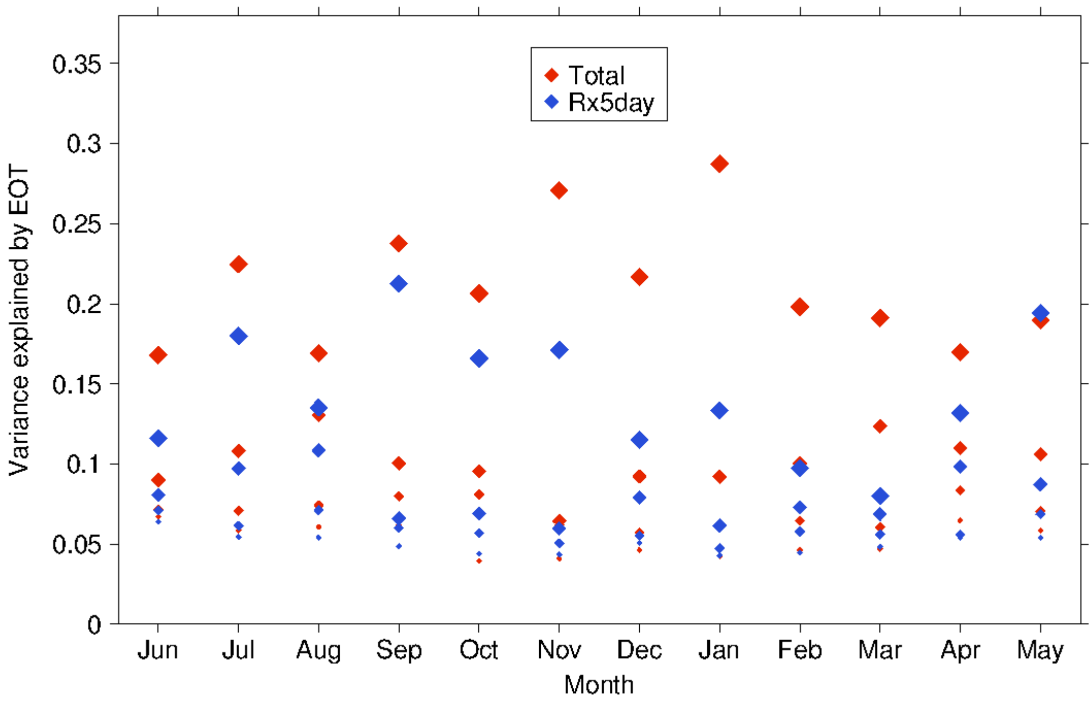

Figure S3: Fraction of total variance explained by each of the first four total (red) and Rx5day (blue) EOTs for each calendar month. The size of the diamond decreases for lower-order EOTs (i.e. the largest diamond represents the first EOT).

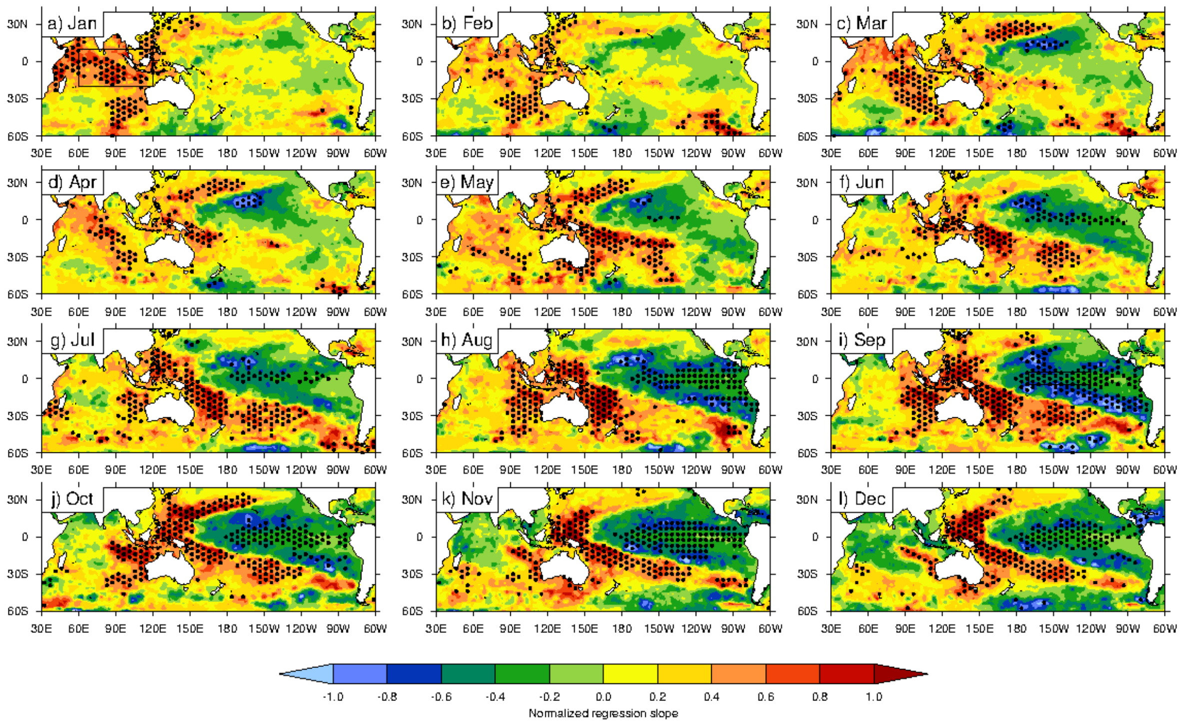

Figure S4: (a-l) As Figure 7 for December total rainfall EOT1.

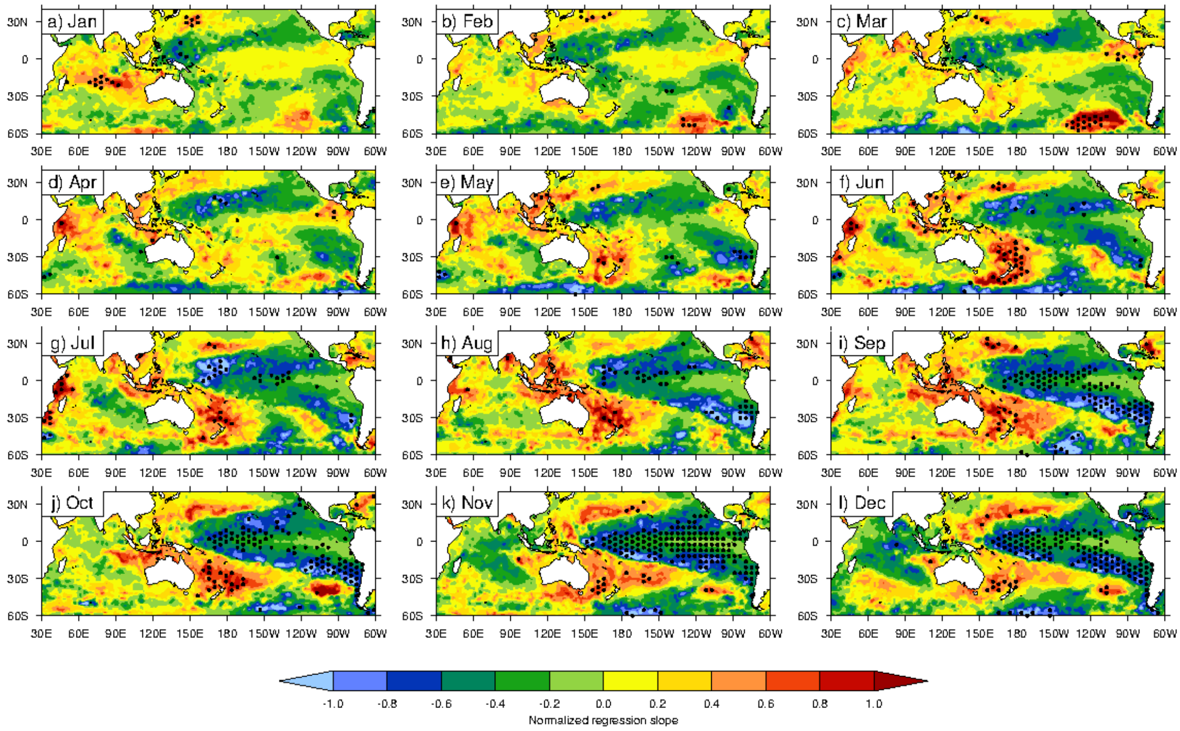

Figure S5: (a-l) As Figure 9 for December total rainfall EOT1.

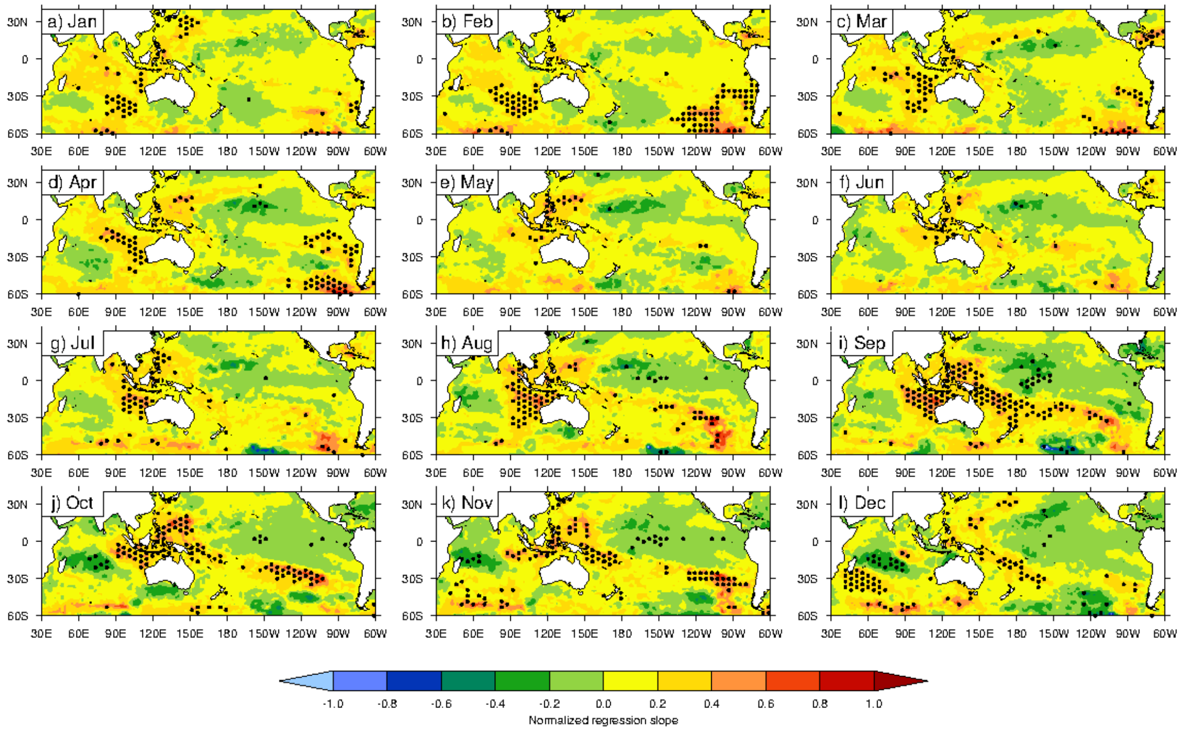

Figure S6: (a-l) As Figure 10 for December total rainfall EOT1.

Supplementary Tables

Table S1: Table showing each four monthly Rx5day EOTs, their locations, the percentage of associated variance, trends, and correlation coefficients with a range of climate indices (SOI, Niño-3.4 index, DMI, SAM index). Locations of EOTs are described by location within each state or territory (New South Wales (NSW), Northern Territory (NT), Queensland (QLD), South Australia (SA), Tasmania (TAS), Victoria (VIC), Western Australia (WA)). All correlation coefficients are computed using Spearman's rank correlations. Significant trends and correlation coefficients at the 5% level are shown in bold text.

EOT	Variance	Location	Trend	SOI	Niño3.4	DMI	DMI (no ENSO)	SAM
June								
EOT1	11.58	NE NSW	-0.06	0.10	-0.13	0.08	0.11	0.22
EOT2	8.09	NW QLD	-0.10	0.11	-0.15	-0.18	-0.15	-0.10
EOT3	7.1	NW WA	-0.10	0.07	0.09	-0.17	-0.19	-0.07
EOT4	6.39	SE NSW	-0.08	0.05	-0.11	-0.08	-0.06	-0.12
July								
EOT1	17.99	S QLD	-0.02	**0.37**	**-0.40**	**-0.27**	-0.18	0.25
EOT2	9.73	W QLD	-0.05	0.10	0.01	0.09	0.09	0.08
EOT3	6.14	NE NSW	-0.15	-0.08	-0.04	-0.05	-0.04	0.09
EOT4	5.44	E QLD	-0.04	-0.11	-0.06	-0.02	0.00	-0.12
August								
EOT1	13.52	SE QLD	0.03	**0.28**	**-0.23**	0.00	0.09	0.22
EOT2	10.84	NE NSW	-0.12	0.07	-0.01	0.06	0.06	0.04
EOT3	7.12	SE NSW	-0.02	0.20	-0.11	-0.16	-0.12	-0.15
EOT4	5.42	C VIC	-0.07	0.21	**-0.23**	-0.12	-0.04	**0.33**
September								
EOT1	21.26	C QLD	0.07	**0.31**	**-0.23**	**-0.35**	**-0.24**	0.19
EOT2	6.61	E QLD	0.11	-0.08	-0.02	0.04	0.05	0.10
EOT3	6.01	C NSW	-0.10	0.02	0.07	0.09	0.05	0.13
EOT4	4.87	E NSW	-0.02	-0.04	-0.09	0.17	0.21	0.19

October								
EOT1	16.58	W QLD	-0.01	**0.39**	**-0.41**	**-0.32**	-0.11	0.21
EOT2	6.91	NE NSW	0.19	0.04	-0.08	0.14	0.18	0.11
EOT3	5.68	C QLD	-0.01	**0.32**	-0.18	-0.14	-0.04	-0.10
EOT4	4.42	SE NSW	-0.12	0.13	-0.06	-0.09	-0.05	0.18
November								
EOT1	17.12	C QLD	0.11	**0.26**	**-0.35**	-0.11	0.04	**0.31**
EOT2	5.98	W NT	0.16	0.17	-0.15	0.01	0.07	0.07
EOT3	5.05	E NSW	0.04	**0.33**	**-0.27**	-0.15	-0.03	0.20
EOT4	4.36	E QLD	0.11	0.15	-0.16	**-0.27**	-0.20	0.07
December								
EOT1	11.49	E QLD	0.28	**0.41**	**-0.41**	-0.09	0.00	-0.01
EOT2	7.9	NE WA	0.43	**0.25**	-0.12	0.00	0.02	0.06
EOT3	5.52	C QLD	-0.06	-0.01	0.00	-0.13	-0.13	-0.16
EOT4	5.08	S NSW	0.10	0.20	-0.07	0.03	0.04	**0.33**
January								
EOT1	13.34	C QLD	0.21	0.15	-0.05	-0.01	-0.01	0.22
EOT2	6.56	C NT	0.28	0.02	0.12	0.17	0.17	0.05
EOT3	4.73	E QLD	-0.23	0.03	-0.02	0.12	0.12	0.03
EOT4	4.3	NW NSW	0.17	-0.01	-0.03	**0.30**	**0.30**	0.01
February								

EOT1	9.76	E NT	0.37	**0.32**	-0.08	**0.29**	**0.28**	0.06
EOT2	7.3	E QLD	0.22	0.21	-0.04	0.12	0.11	0.15
EOT3	5.78	NE WA	0.19	0.15	-0.13	0.07	0.04	0.05
EOT4	4.48	N QLD	-0.19	0.02	0.07	0.13	0.15	0.18
March								
EOT1	8	N QLD	0.20	**0.29**	-0.10	0.08	0.05	0.21
EOT2	6.87	NE WA	**0.72**	0.08	-0.18	0.11	0.07	0.14
EOT3	5.61	SW QLD	0.03	0.04	0.03	0.21	**0.22**	0.08
EOT4	4.85	N NT	-0.07	0.13	-0.09	0.05	0.02	**0.30**
April								
EOT1	13.17	SW QLD	0.17	**0.30**	**-0.25**	-0.01	-0.04	0.04
EOT2	9.84	N NT	-0.02	**0.39**	-0.15	0.17	0.15	0.14
EOT3	5.59	N WA	0.21	-0.02	0.02	-0.17	-0.17	0.08
EOT4	5.42	E QLD	-0.14	-0.04	0.02	-0.20	-0.19	-0.03
May								
EOT1	19.43	E QLD	0.08	**0.34**	-0.13	-0.20	-0.19	0.08
EOT2	8.74	W QLD	-0.11	**0.27**	0.00	**-0.35**	**-0.35**	-0.19
EOT3	6.87	NE NSW	0.09	0.16	0.09	0.04	0.03	0.01
EOT4	5.4	NW WA	-0.11	-0.02	0.03	-0.02	-0.02	0.13

Table S2: As Table S1 except for monthly total rainfall EOTs.

EOT	Variance	Location	Trend	SOI	Niño3.4	DMI	DMI (no ENSO)	SAM
June								
EOT1	16.79	NE NSW	-0.14	**0.23**	-0.17	0.05	0.08	**0.28**
EOT2	9	W VIC	-0.02	0.20	0.01	-0.11	-0.11	-0.13
EOT3	7.16	W WA	-0.02	0.07	-0.11	0.01	0.03	-0.16
EOT4	6.73	E NSW	-0.22	0.05	0.10	-0.06	-0.08	0.08
July								
EOT1	22.47	S QLD	-0.07	**0.41**	**-0.43**	**-0.26**	-0.17	**0.27**
EOT2	10.82	SE NSW	0.00	**0.31**	-0.13	-0.11	-0.07	**-0.34**
EOT3	7.08	E NT	0.05	-0.05	0.16	0.12	0.08	0.07
EOT4	5.86	W WA	0.17	0.10	-0.01	-0.09	-0.08	-0.12
August								
EOT1	16.92	E VIC	-0.29	**0.25**	**-0.24**	**-0.35**	**-0.27**	0.01
EOT2	13.05	SE QLD	-0.13	**0.33**	-0.19	0.04	0.11	0.19
EOT3	7.42	W TAS	0.32	0.11	-0.16	-0.18	-0.13	-0.14
EOT4	6.07	E NSW	-0.03	0.09	-0.07	0.00	0.03	0.05
September								
EOT1	23.77	C QLD	0.17	**0.38**	**-0.36**	**-0.29**	-0.11	**0.28**
EOT2	10.03	E VIC	0.14	0.10	0.04	**-0.24**	**-0.26**	0.01
EOT3	7.98	W TAS	0.26	0.16	0.02	-0.12	-0.13	**-0.53**
EOT4	6.19	NE NSW	0.00	0.07	-0.03	-0.10	-0.08	-0.03

October								
EOT1	20.64	SE NSW	-0.28	**0.41**	**-0.32**	**-0.37**	-0.20	0.21
EOT2	9.53	SE QLD	0.11	0.11	-0.12	0.10	0.16	0.09
EOT3	8.1	C QLD	0.06	**0.25**	**-0.34**	**-0.26**	-0.08	0.03
EOT4	3.96	NW TAS	-0.03	0.22	-0.17	-0.17	-0.08	**-0.43**
November								
EOT1	27.07	C QLD	**0.42**	**0.35**	**-0.41**	**-0.24**	-0.06	**0.33**
EOT2	6.46	NE NT	-0.02	**0.27**	**-0.30**	-0.10	0.03	0.24
EOT3	6.2	SE NSW	0.05	**0.24**	-0.21	-0.02	0.08	0.00
EOT4	4.11	SE QLD	-0.21	0.09	0.03	-0.06	-0.07	0.05
December								
EOT1	21.69	N QLD	**0.86**	**0.46**	**-0.34**	-0.10	-0.03	0.22
EOT2	9.23	NW NT	**0.61**	0.07	0.02	0.02	0.02	0.02
EOT3	5.74	C NSW	0.22	0.11	0.00	-0.09	-0.09	**0.28**
EOT4	4.64	E QLD	0.17	0.08	-0.16	-0.08	-0.04	-0.24
January								
EOT1	28.74	C QLD	0.74	0.15	0.00	0.16	0.16	**0.27**
EOT2	9.21	NW NT	**1.24**	0.12	0.00	0.06	0.06	0.23
EOT3	6.25	NE QLD	-1.02	**0.23**	-0.19	0.03	0.03	0.10
EOT4	4.25	NW NSW	-0.05	-0.07	-0.05	0.17	0.17	-0.03
February								

EOT1	19.81	N NT	**1.36**	**0.54**	**-0.30**	0.21	0.15	0.07
EOT2	10.02	E QLD	-0.89	0.08	-0.08	0.13	0.11	0.19
EOT3	6.45	NW QLD	-0.08	0.17	-0.01	0.18	0.18	0.07
EOT4	4.64	N QLD	0.68	0.13	-0.11	0.13	0.10	0.08
March								
EOT1	19.11	NW NT	**1.39**	**0.42**	**-0.38**	0.06	-0.05	0.19
EOT2	12.36	NE QLD	-0.78	**0.32**	-0.15	0.08	0.04	0.15
EOT3	6.06	S QLD	0.09	0.06	-0.04	0.14	0.14	0.05
EOT4	4.7	NE WA	0.51	-0.13	0.09	0.03	0.05	-0.02
April								
EOT1	16.97	E QLD	0.20	**0.23**	-0.18	0.10	0.08	0.06
EOT2	11.01	N NT	0.35	**0.29**	-0.11	0.16	0.15	0.14
EOT3	8.35	E NSW	-0.38	**0.28**	**-0.26**	-0.04	-0.07	-0.09
EOT4	6.47	N QLD	0.00	**0.28**	-0.20	0.14	0.12	-0.06
May								
EOT1	18.97	E QLD	-0.01	**0.37**	-0.14	**-0.28**	**-0.26**	0.17
EOT2	10.61	N VIC	-0.05	**0.38**	-0.06	-0.19	-0.18	-0.12
EOT3	7.07	NE NSW	0.15	-0.06	0.13	0.20	0.18	0.16
EOT4	5.85	SW WA	0.03	0.01	-0.08	-0.07	-0.06	0.05

Table S3: Table showing each four monthly Rx5day EOTs, their locations, the percentage of associated variance, and correlation coefficients with a range of climate indices (Blocking index, STR position index, STR intensity index, SPCZ index, Tropical Cyclone (West) index, Tropical Cyclone (East) index). Locations of EOTs are described by location within each state or territory (New South Wales (NSW), Northern Territory (NT), Queensland (QLD), South Australia (SA), Tasmania (TAS), Victoria (VIC), Western Australia (WA)). All correlation coefficients are computed using Spearman's rank correlations. Significant correlation coefficients at the 5% level are shown in bold text.

EOT	Variance	Location	BI	STR-P	STR-I	SPCZ-I	TC-W	TC-E
June								
EOT1	11.58	NE NSW	0.02	-0.15	-0.08	-0.05		
EOT2	8.09	NW QLD	0.11	-0.02	-0.09	0.01		
EOT3	7.1	NW WA	0.18	0.07	-0.20	0.08		
EOT4	6.39	SE NSW	**0.23**	0.02	-0.16	-0.05		
July								
EOT1	17.99	S QLD	0.20	**-0.32**	0.04	-0.15		
EOT2	9.73	W QLD	0.21	0.21	-0.15	-0.11		
EOT3	6.14	NE NSW	-0.12	0.01	-0.04	0.05		
EOT4	5.44	E QLD	0.11	0.07	-0.10	0.19		
August								
EOT1	13.52	SE QLD	**0.27**	-0.18	0.03	0.04		
EOT2	10.84	NE NSW	0.18	-0.19	0.04	0.12		

EOT3	7.12	SE NSW	**0.40**	**0.23**	**-0.41**	0.02		
EOT4	5.42	C VIC	**0.42**	0.12	**-0.26**	0.04		
September								
EOT1	21.26	C QLD	**0.30**	0.07	-0.19	-0.10		
EOT2	6.61	E QLD	**0.23**	-0.02	0.08	0.13		
EOT3	6.01	C NSW	**0.32**	0.05	-0.18	0.14		
EOT4	4.87	E NSW	-0.09	**-0.36**	**0.30**	-0.03		
October								
EOT1	16.58	W QLD	**0.24**	0.21	**-0.24**	-0.04		
EOT2	6.91	NE NSW	0.06	**-0.31**	0.14	-0.07		
EOT3	5.68	C QLD	0.16	0.06	-0.13	0.06		
EOT4	4.42	SE NSW	**0.36**	**-0.29**	-0.07	0.17		
November								
EOT1	17.12	C QLD	**0.31**	**-0.37**	0.18	-0.08	0.15	-0.03
EOT2	5.98	W NT	-0.06	0.12	-0.09	-0.06	0.16	0.16
EOT3	5.05	E NSW	0.16	-0.15	0.11	-0.07	0.11	0.10
EOT4	4.36	E QLD	0.14	0.05	-0.10	-0.12	0.15	0.01
December								
EOT1	11.49	E QLD	-0.11	-0.05	-0.15	**-0.23**	**0.33**	**0.32**
EOT2	7.9	NE WA	-0.21	0.14	**-0.25**	**-0.24**	**0.42**	-0.12

EOT3	5.52	C QLD	-0.08	0.08	0.01	0.11	0.16	0.03
EOT4	5.08	S NSW	0.19	-0.17	0.14	-0.11	0.02	0.03
January								
EOT1	13.34	C QLD	-0.13	0.00	-0.18	-0.21	0.05	0.17
EOT2	6.56	C NT	**-0.23**	0.00	-0.07	0.13	**0.29**	-0.16
EOT3	4.73	E QLD	0.09	-0.04	-0.03	0.20	-0.08	-0.04
EOT4	4.3	NW NSW	0.17	-0.18	**0.25**	0.09	-0.06	-0.06
February								
EOT1	9.76	E NT	**-0.26**	-0.10	-0.10	-0.11	0.11	-0.05
EOT2	7.3	E QLD	-0.06	-0.27	0.17	-0.06	-0.17	0.08
EOT3	5.78	NE WA	-0.10	0.03	-0.16	-0.09	**0.41**	-0.01
EOT4	4.48	N QLD	0.07	-0.01	0.00	-0.09	-0.01	0.02
March								
EOT1	8	N QLD	-0.09	**-0.22**	0.18	**-0.25**	0.10	0.10
EOT2	6.87	NE WA	0.12	-0.07	0.01	-0.10	**0.34**	-0.06
EOT3	5.61	SW QLD	0.17	-0.04	0.10	0.05	-0.20	-0.04
EOT4	4.85	N NT	0.04	-0.15	0.13	-0.03	**0.45**	0.14
April								
EOT1	13.17	SW QLD	0.08	-0.05	-0.06	-0.05	0.15	-0.07
EOT2	9.84	N NT	0.05	-0.01	0.01	**-0.22**	**0.43**	0.11
EOT3	5.59	N WA	0.19	-0.13	0.02	0.11	0.13	0.09

EOT4	5.42	E QLD	-0.02	-0.03	-0.02	0.14	-0.02	**0.26**
May								
EOT1	19.43	E QLD	0.06	-0.10	-0.07	0.05		
EOT2	8.74	W QLD	**0.30**	**0.25**	**-0.42**	0.13		
EOT3	6.87	NE NSW	0.21	0.02	-0.10	0.08		
EOT4	5.4	NW WA	0.14	0.11	-0.12	0.13		

Table S4: As Table S3 except for monthly total rainfall EOTs.

EOT	**Variance**	**Location**	**BI**	**STR-P**	**STR-I**	**SPCZ-I**	**TC-W**	**TC-E**
June								
EOT1	16.79	NE NSW	0.21	-0.07	-0.21	-0.05		
EOT2	9	W VIC	**0.26**	**0.60**	**-0.50**	0.15		
EOT3	7.16	W WA	**0.37**	0.02	-0.21	0.01		
EOT4	6.73	E NSW	0.06	0.00	-0.16	0.08		
July								
EOT1	22.47	S QLD	**0.23**	**-0.28**	0.00	-0.21		
EOT2	10.82	SE NSW	**0.27**	**0.61**	**-0.58**	0.16		
EOT3	7.08	E NT	-0.05	-0.06	0.18	**-0.24**		
EOT4	5.86	W WA	0.07	0.12	**-0.29**	0.12		
August								
EOT1	16.92	E VIC	**0.33**	**0.47**	**-0.54**	0.13		

EOT2	13.05	SE QLD	**0.39**	-0.06	-0.14	0.08		
EOT3	7.42	W TAS	**-0.52**	0.05	0.03	-0.04		
EOT4	6.07	E NSW	0.02	0.09	-0.16	0.04		
September								
EOT1	23.77	C QLD	**0.27**	-0.07	-0.14	-0.16		
EOT2	10.03	E VIC	**0.38**	**0.34**	**-0.35**	0.19		
EOT3	7.98	W TAS	**-0.43**	**0.42**	**-0.25**	-0.10		
EOT4	6.19	NE NSW	0.04	0.14	-0.21	0.04		
October								
EOT1	20.64	SE NSW	**0.46**	0.19	**-0.33**	0.05		
EOT2	9.53	SE QLD	0.13	-0.19	0.04	-0.10		
EOT3	8.1	C QLD	-0.11	0.06	0.01	-0.18		
EOT4	3.96	NW TAS	-0.02	**0.66**	**-0.36**	-0.01		
November								
EOT1	27.07	C QLD	**0.38**	**-0.27**	0.07	-0.15	0.21	-0.05
EOT2	6.46	NE NT	**0.28**	-0.09	-0.03	-0.03	**0.36**	0.16
EOT3	6.2	SE NSW	-0.07	-0.06	0.11	-0.07	-0.02	0.14
EOT4	4.11	SE QLD	**0.24**	**-0.32**	0.27	0.08	0.03	0.14
December								
EOT1	21.69	N QLD	-0.05	0.06	-0.20	-0.16	**0.50**	**0.25**

EOT2	9.23	NW NT	-0.16	-0.12	0.01	-0.03	0.21	-0.20
EOT3	5.74	C NSW	**0.23**	**-0.39**	**0.23**	-0.12	-0.04	-0.03
EOT4	4.64	E QLD	-0.13	0.07	-0.16	-0.03	0.01	0.08
January								
EOT1	28.74	C QLD	-0.05	-0.09	-0.11	-0.18	0.07	0.08
EOT2	9.21	NW NT	-0.16	-0.02	-0.13	-0.06	**0.30**	-0.11
EOT3	6.25	NE QLD	-0.19	-0.07	0.00	-0.14	0.02	**0.26**
EOT4	4.25	NW NSW	**0.23**	-0.21	0.12	0.03	-0.05	0.06
February								
EOT1	19.81	N NT	**-0.26**	-0.10	-0.20	-0.20	**0.29**	0.11
EOT2	10.02	E QLD	0.03	**-0.23**	0.04	-0.07	**-0.22**	0.07
EOT3	6.45	NW QLD	-0.06	-0.02	0.06	0.00	-0.08	0.04
EOT4	4.64	N QLD	-0.01	-0.11	-0.01	**-0.24**	0.15	0.12
March								
EOT1	19.11	NW NT	-0.07	-0.15	0.03	-0.21	**0.49**	0.07
EOT2	12.36	NE QLD	-0.07	-0.21	0.04	-0.13	**0.24**	**0.35**
EOT3	6.06	S QLD	**0.27**	-0.05	0.00	0.11	-0.06	-0.21
EOT4	4.7	NE WA	0.06	0.08	-0.06	-0.04	-0.05	**-0.26**
April								
EOT1	16.97	E QLD	0.06	-0.07	0.08	0.02	0.14	0.08
EOT2	11.01	N NT	-0.01	0.13	-0.15	-0.21	**0.49**	0.09

EOT3	8.35	E NSW	**0.27**	**-0.28**	-0.04	-0.14	-0.14	-0.10
EOT4	6.47	N QLD	-0.01	-0.02	0.13	**-0.30**	0.15	**0.27**
May								
EOT1	18.97	E QLD	**0.25**	-0.13	-0.13	0.08		
EOT2	10.61	N VIC	**0.27**	0.41	**-0.45**	0.18		
EOT3	7.07	NE NSW	0.20	-0.24	0.11	-0.01		
EOT4	5.85	SW WA	0.17	0.12	**-0.39**	0.02		